ADO746343

AFML-TR-72-20

FATIGUE-CRACK PROPAGATION IN D6AC STEEL PLATE FOR SEVERAL FLIGHT LOADING PROFILES IN DRY AIR AND JP-4 FUEL ENVIRONMENTS

Charles E. Feddersen

BATTELLE
Columbus Laboratories

TECHNICAL REPORT AFML-TR-72-20
January 1972

APPROVED FOR PUBLIC RELEASE; DISTRIBUTION UNLIMITED.

AIR FORCE MATERIALS LABORATORY
AIR FORCE SYSTEMS COMMAND
WRIGHT-PATTERSON AIR FORCE BASE, OHIO

NOTICE

AD746343

AFML-TR-72-20

FATIGUE-CRACK PROPAGATION IN D6AC STEEL PLATE FOR SEVERAL FLIGHT LOADING PROFILES IN DRY AIR AND JP-4 FUEL ENVIRONMENTS

by

Charles E. Feddersen

FOREWORD

This program was conducted in support of the F-111 Recovery Effort to evaluate fatigue crack propagation rates in high strength D6AC steel plate under selected cyclic load and environmental conditions. This research task has been conducted by the Structural Materials Division, Engineering Systems Department of Battelle's Columbus Laboratories, Columbus, Ohio. The program was sponsored by the Air Force Materials Laboratory, Air Force Systems Command, Wright-Patterson Air Force Base, Ohio, through the University of Dayton Research Institute, Dayton, Ohio, under Subcontract No. 71-5 to Contract No. F33615-71-C-1054. Mr. Clayton L. Harmsworth , LAE, of the Air Force Materials Laboratory provided technical liaison. This report summarizes work performed during the period from February 23, 1971, to October 31, 1971.

The experimental portions of this research program were conducted in Battelle's Structural Engineering Laboratory under the direction of Henry J. Malik, Laboratory Supervisor. The structural testing was performed by James F. Wood and Wilbur L. Mefford. The load profile control was prepared by Dennis G. Rider.

This technical report has been reviewed and is approved.

Albert Olevitch

Albert Olevitch
Chief, Materials Engineering Branch
Materials Support Division
Air Force Materials Laboratory

ABSTRACT

The objective of this experimental program was to obtain an independent evaluation of the fatigue-crack propagation characteristics of D6AC steel for the F-111 aircraft under specific flight loading spectra. The program also included selected studies of constant amplitude fatigue-crack propagation and crack growth retardation under the influence of single overloads.

It was determined that fatigue-crack propagation specimens evaluated under spectra with peak loads exceeding one-half of the tensile yield strength of the material sustained significantly longer lifetimes than under spectra wherein the peak loads were significantly below this stress level. An upper limit to this beneficial behavior was not established. It was noted that the distribution of the peak loads were also a significant factor in retarding crack growth.

Although the observations were limited, an effect of maximum cyclic stress on constant amplitude crack growth rates was apparent. In the crack growth retardation studies, it was observed that the overload ratio plays a direct role and the maximum cyclic stress level plays an inverse role in delaying crack growth.

Prediction of crack growth curves for variable amplitude flight profile loadings was attempted by using various crack growth rate integration routines on constant amplitude fatigue-crack propagation data. However, the sensitivity of these routines to both initial crack size and terminal toughness was generally greater than the accuracy to which these quantities were known. It was noted that a more meaningful appraisal and comparison of loading spectra could be achieved by a rate analysis of crack growth in terms of flight profiles rather than by the prediction of crack growth in terms of a retardation parameter strongly influenced both by initial crack size and by terminal toughness.

TABLE OF CONTENTS

TABLE OF CONTENTS
(Continued)

APPENDIX A

APPENDIX B

LIST OF TABLES

LIST OF FIGURES

LIST OF FIGURES
(Continued)

LIST OF SYMBOLS

A	Calibration factor for crack compliance
B	Specimen thickness, inches
C	Parametric coefficient in Paris model of fatigue-crack propagation
COD	Crack opening displacement at mouth of starter notch, inches
E	Young's elastic modulus
K	Stress intensity factor, ksi-in$^{1/2}$
ΔK	Stress intensity factor range, ksi-in$^{1/2}$
N	Number of cycles
N_p	Number of profiles
N_r	Number of cycles retarded
Q	Plasticity corrected shape factor
S	Gross stress, ksi
T	Flight time, hours
W	Specimen width, inches
$\varkappa_o$	Displacement of center of crack surface from reference axis
μ	Poisson's ratio
Φ	Surface flaw shape factor
a	Surface crack depth into specimen thickness, inches
c	Half crack length for surface crack or through crack, inches
m	Retardation parameter in Wheeler model
n	Parametric exponent in Paris rate model of fatigue and propagation

I. – INTRODUCTION

In support of the F-111 aircraft recovery effort, the Air Force Materials Laboratory requested that Battelle's Columbus Laboratories conduct an experimental program to develop supplementary fatigue-crack propagation information on D6AC steel plate. This program was concerned primarily with developing fatigue-crack propagation information on specific flight loading spectra in dry air (as a reference) and water-saturated JP-4 fuel environments. This information was developed as an independent evaluation of the spectrum load effects which were being studied by the Convair Aerospace Division of General Dynamics Corporation, but which were not being duplicated elsewhere in the multilaboratory experimental program. For purposes of experimental correlation, a limited amount of constant amplitude fatigue-crack propagation and some exploratory crack growth retardation studies were also included.

II.– PROGRAM DESCRIPTION

The experimental program considered three types of fatigue-crack propagation (FCP) studies on surface flaws in D6AC steel plate, namely,

(1) the determination of constant amplitude FCP behavior

(2) the determination of FCP behavior under specific flight loading profiles

(3) the determination of the effect of single overloads on constant amplitude FCP.

The overall test matrix is presented in Table 1.

The initial task provided reference or baseline FCP data for purposes of experimental correlation. Three different maximum cyclic stress levels and two different frequencies were considered in an attempt to discern further detailed influences of these variables. The environment and stress ratio were limited to singular conditions since their influence has been determined more positively elsewhere.[(1)*]

The second and principal task provided a comparative evaluation of specific flight load spectrum effects. The Air Force Materials Laboratory, in

---

*References are listed on Page 44.

TABLE I. EXPERIMENTAL TEST MATRIX

Experimental Task	Specimen Number	Test Environment	Thickness B inch	Width W inch	Cyclic Loading Conditions: Maximum Cyclic Stress S_{max} ksi	Cyclic Loading Conditions: Stress Ratio R	Frequency Hz
Constant Amplitude Fatigue Crack Propagation	1	Desiccated Air	.607	6.00	40	0.1	3
	18	Desiccated Air	.292	6.01	40	0.1	8
	5	Desiccated Air	.609	6.01	60	0.1	3
	2	Desiccated Air	.606	6.01	100	0.1	3
					Flight Spectrum[a]		
Fatigue Crack Propagation Under Flight Loading Profiles	3	Desiccated Air	.605	6.01	5g MAC		3
	6	Water Saturated JP-4	.608	6.01	5g MAC		2
	9	Water Saturated JP-4	.602	6.01	5g MAC w/comp		2
	4	Desiccated Air	.590	6.01	7.33g MAC		3
	8	Water Saturated JP-4	.602	5.99	7.33g MAC		2
	10	Water Saturated JP-4	.598	6.01	5g CTB		2
	11	Desiccated Air	.284	6.01	3g FB		3
	12	Water Saturated JP-4	.284	6.01	3g FB		2
					Maximum Cyclic Stress S_{max} ksi	Overload Ratio OR	
Effect of Single Overloads	17	Desiccated Air	.295	6.01	40	1.70	8
	13	Desiccated Air	.278	6.00	40	1.35	8
	14	Desiccated Air	.286	6.00	40	-0.35	8
	15	Desiccated Air	.603	6.02	40	1.70	8
	22	Desiccated Air	.594	6.01	40	1.35	8
	16	Desiccated Air	.606	6.00	40	-0.35	8
	20	Desiccated Air	.603	6.00	80, 60, 40	1.70	3
	19	Desiccated Air	.603	6.01	80, 60	1.35	3
	21	Desiccated Air	.603	6.00	80	-0.35	3

(a) See Appendix A for spectra details.

conjunction with the principal members of the Inspection Interval Task Group of the Air Force Scientific Advisory Board, specified these flight loading profiles as the most significant for an independent evaluation of the crack propagation behavior of the D6AC steel plate material being used in the F-111 aircraft. Because program scheduling necessitated time compression, only a minimal allowance for time dependency of environmental effects was permitted. The desiccated air (as a neutral reference environment) tests were conducted at a cyclic rate of 3 Hz; the water-saturated JP-4 tests at 2 Hz.

The third and final task provided exploratory information on the influence of single overloads on constant amplitude fatigue-crack propagation behavior. This information was developed to provide more insight into the nature of crack growth retardation.

III. – EXPERIMENTAL DETAILS

The fatigue-crack propagation studies of this program were conducted in Battelle-Columbus' Structural Engineering Laboratory. The test specimens were manufactured by the Convair Aerospace Division of General Dynamics in accordance with specified U. S. Air Force and General Dynamics production procedures for the F-111 aircraft. This assured that the test specimens were representative of F-111 aircraft structural components. It also eliminated specimen manufacture as a variable in the eventual correlation of these fatigue-crack propagation results.

Materials

The material used in this experimental program was obtained from F-111 production lots of D6AC steel plate at General Dynamics. The material was processed in a nominal thickness of 0.8 inch and in plate sizes of 2 x 3 or 3 x 3 feet to simulate component sizes. These plates were heat treated along with production materials and then machined into test specimens.

Heat Treatment

The specimen materials used in this program were included or "piggybacked" with three different production runs in the following heat treatment.

The plates were furnace austenitized at a temperature of 1700 F ($\pm$ 25 F) and then "Aus-Bay" quenched in the furnace to a temperature of 975 F ($\pm$ 25 F). (The "Aus-Bay" region is that portion of the time-temperature transformation diagram below the pearlitic nose where the austenitic microstructure may be retained for a relatively long period of time without transformation into other products such as ferrite, pearlite, bainite, or others.) Following "Aus-Bay" temperature equalization, all plate and forging elements were quenched in the 140 F $\pm$ 10 F oil. They were subject to a snap draw at 370 F. Finally, they were double tempered between 1000 F and 1025 F for a minimum of 2 hours actual soak time at temperature. They were air-cooled to room temperature between and after the tempering stages.

Reference Mechanical Properties

To qualify the mechanical properties of this material, from one to four tensile specimens were tested from each heat-treatment lot. Fracture toughness was evaluated with two compact tension tests from each plate piece. All specimens were cut from the central region of the plate pieces. The tensile and fracture toughness properties are summarized in Tables II and III, respectively.

Although this material was originally specified as a high-toughness grade (K_{Ic} = 90 $\pm$ 10 ksi-in$^{1/2}$) of D6AC plate, it can be seen from Table III that this requirement is barely satisfied at an average room temperature level of 80 ksi-in$^{1/2}$. In evaluating crack lifetimes under various flight loading spectra later in this report, it should be borne in mind that the toughness level is at the lower bound of the specified range.

Specimen Preparation

Following heat treatment, test specimens were machined to the configuration shown in Figure 1 in two nominal thicknesses, 0.28 and 0.60 inches. Depending on plate size, either two or three specimens were obtained from each plate. The specimens were shot-peened, cadmium plated, and painted prior to shipping from General Dynamics Corporation. Upon receipt at Battelle-Columbus, two starter notches symmetrically spaced 6 inches apart on the specimen center-line were electrical-discharge-machined (EDM) into one surface of the reduced

TABLE II. SUMMARY OF ROOM-TEMPERATURE TENSILE PROPERTIES (DATA DERIVED BY GENERAL DYNAMICS CORPORATION)

Heat Treat Lot No.	GD Tensile Specimen No.	Tensile Ultimate Strength, ksi	0.2% Tensile Yield Strength, ksi	Elongation in 2-inch Gage Length, percent	Reduction in Area, percent
15B	AIR4	229.0	205.8	10.7	39.0
15B	AIR5	225.8	201.8	10.7	39.8
16B	BIS4	230.1	207.1	11.4	45.6
20B	BIR5	238.6	217.7	11.4	41.6
20B	DIS4	237.0	214.4	11.4	40.3
20B	E2R7	227.5	204.2	12.1	44.3
20B	E2T7	231.4	207.6	10.7	42.0
Average		231.3	208.4	11.2	41.8

TABLE III. SUMMARY OF COMPACT TENSION FRACTURE TOUGHNESS TESTS (DATA DERIVED BY GENERAL DYNAMICS CORP.)

Heat Treat Lot No.	GD Specimen No.	Test Temperature, F		Fracture Toughness, K_{Ic}, ksi-in.$^{1/2}$
15B	A1R6	70		73.9
	A1R8	70		77.7
	C1S4	70		80.4
	C1S6	70		80.9
			Average	78.2
16B	B1S7	70		85.8
	B1S11	70		84.7
	C1R8	70		77.1
	C1R9	70		77.9
			Average	81.4
20B	A1S4	70		80.6
	A1S6	70		85.1
	B1R7	70		75.3
	B1R11	70		75.6
	D1R4	70		87.5
	D1R6	70		84.5
	D1S6	70		80.3
	D1S8	70		78.3
			Average	80.9
20B	E2R8	-40		59.2
	E2R10	-40		60.5
	E2S6	-40		71.4
	E2S8	-40		57.9
	E2T8	-40		66.3
	E2T10	-40		58.4
			Average	62.3

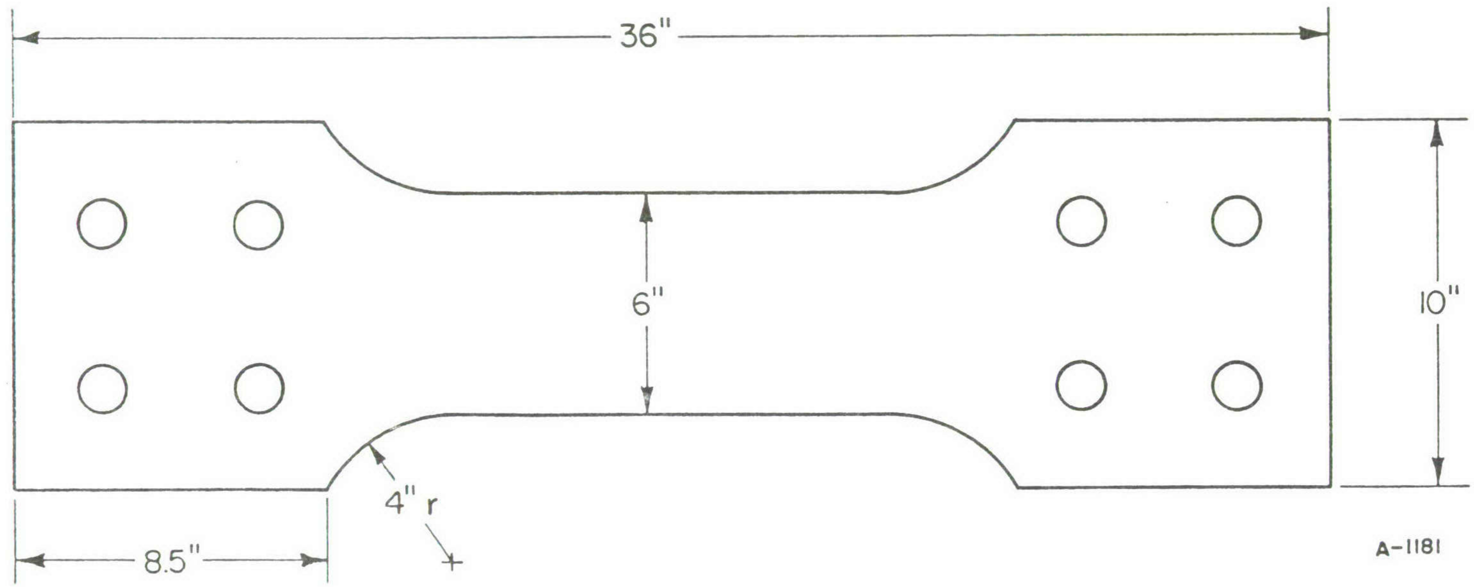

FIGURE 1. PLANFORM OF SURFACE FLAW TEST SPECIMEN

section in the Machine Shop. They were then transferred to the Structural Engineering Laboratory for evaluation.

General Testing Procedures

The EDM notched-test specimens were mounted in servocontrolled electrohydraulic testing systems for fatigue precracking and subsequent testing. The typical experimental setup is illustrated in Figure 2.

The specimen is shown mounted between special adapter plates to provide buckling restraint during the compressive cycles. Each specimen contains two surface flaws in the central portion of the reduced section. An environmental chamber (containing, in this case, water-saturated JP-4 fuel) is shown surrounding each flaw. A miniaturized compliance gage is contained in the notch opening of the flaw.

The continuous strip chart recorders and associated readout electronics are shown in the foreground of Figure 2. A digital voltmeter was provided for monitoring load levels during initial calibrations.

A close-up view of the environmental chambers and contained compliance gages is shown in Figure 3. A drop of distilled water is visible at the bottom of each chamber to maintain the water saturation of the JP-4 aircraft fuel.

Precracking was accomplished at a stress level of 60 ksi to generate an initial crack approximately 0.080 inch deep. Upon completion of precracking, the main fatigue-crack propagation test was controlled either by the testing system function generator for the constant amplitude tests, or by a paper-tape-driven digital profiler for the flight simulation loading tests. All tests were conducted under load control, the results of which are presented in the next section of this report.

Special Note. In preparation for the flight load simulation tests, it was noted that even the precracking stress levels did influence the subsequent crack behavior under variable amplitude cycling. While precracking at a relatively high stress (60 ksi) was necessary to initiate a fatigue crack, the subsequent number of loading profiles required to stabilize the continue this growth was quite variable. This is attributed to the variety of load distributions which were contained in the different spectrum profiles. In order to place the resultant crack growth behavior on a common basis, lifetimes were not evaluated relative to a given precrack size, but rather to a larger crack size at which positive regular growth was observed from the compliance record. This reference size was about twice initial notch size or about 0.120 inch in depth.

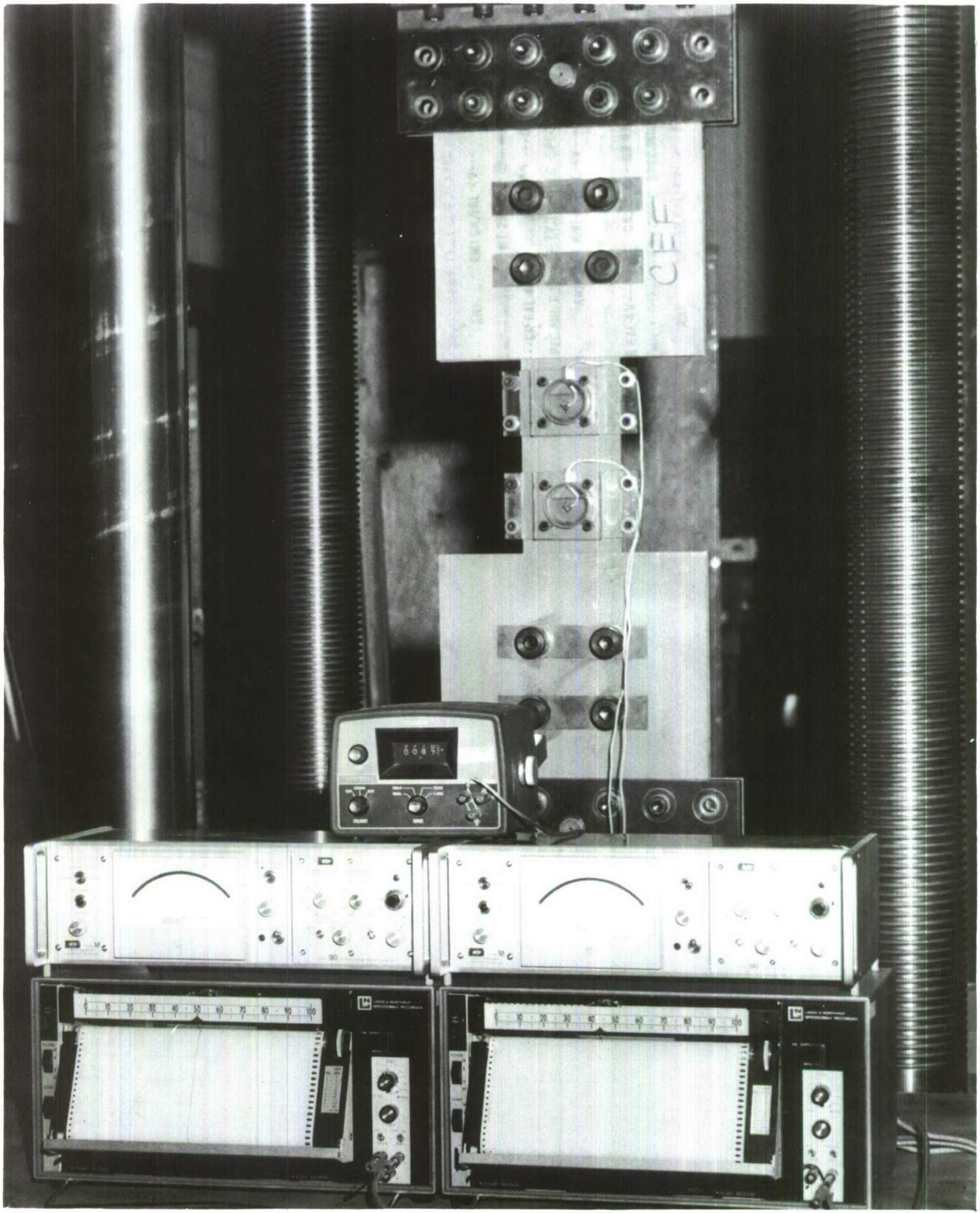

FIGURE 2. TYPICAL FATIGUE-CRACK PROPAGATION TEST SETUP

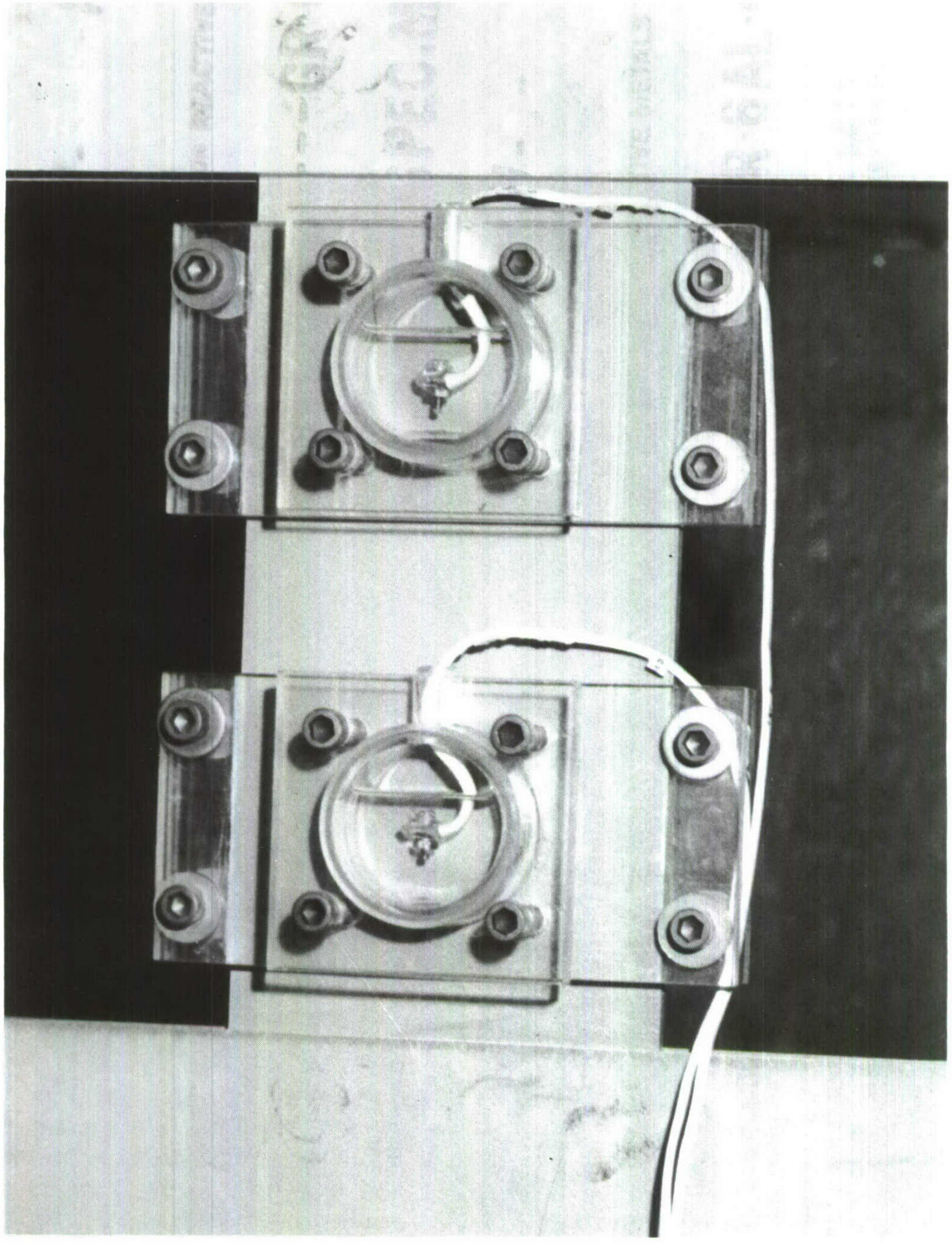

FIGURE 3. CLOSE-UP VIEW OF ENVIRONMENTAL CHAMBERS AND COMPLIANCE GAGES

Environmental Conditions

Two environments were specified for study in this experimental program. Dry or desiccated air was used as the reference environment. This environment was developed by surrounding the flawed or cracked region with an environmental chamber containing anhydrous calcium sulphate as a desiccant. This yielded a relative humidity level of less than 5 percent. The service environment was simulated by submerging the flaw in water-saturated JP-4 fuel, standardized by General Dynamics. Water saturation was assured by maintaining a visible bubble of distilled water within the environmental chamber.

Flight Simulation Loading Profiles

The flight loading spectra used in this program were selected from those developed by the Convair Aerospace Division of General Dynamics for the F-111 aircraft and applied in their fatigue-crack propagation studies. The details of these spectra are presented in Appendix A and are briefly summarized in Table IV. This summary is presented as a coarse characterization of the spectra. Since it was beyond the scope of this program to evaluate the various energy or power parameters which may be associated with such loading spectra, only the extreme applied stresses, the number of cycles, and the associated flight times have been considered.

Stress-Intensity Factor Formulations

The stress-intensity factor formulations which were used in this program are based on the concepts of Irwin.[2,3] For the surface flaw configuration, the stress-intensity factor is expressed as

$$K = 1.1\, S\sqrt{\pi a/Q} \quad , \qquad (1)$$

where

$$Q = \Phi^2 - \frac{S^2}{4\sqrt{2}\,(TYS)^2} \quad ,$$

represents the shape factor modified for plastic zone size, and

Φ = shape factor, elliptic integral of the second kind with modulus, k

$k = \sqrt{1 - a^2/c^2}$

TYS = tensile yield strength of the material.

TABLE IV. FLIGHT SIMULATION LOADING PROFILES

Flight Loading Profile	Maximum Cyclic Stress, S_{max}, ksi	Minimum Cyclic Stress, S_{min}, ksi	Flight Hours per Profile, T, Hrs	Cycles per Profile, N_p
5g MAC	106.6	0.0	200	17241
5g w/comp	108.3	-28.0	200	17270
7.33g MAC	106.7	0.0	200	17239
5g CTB	113.8	0.0	200	16756
3g FB	66.4*	- 5.5	5.25	2508

* Additional overload cycles of 80.3, 78.5, 75.9, 75.2 and 67.7 ksi and a negative excursion of -12.4 ksi are contained in make-up flights following each 20 basic flight profiles. See Appendix A.

Where breakthrough of the surface flaw ass encountered, the center-crack formulation of stress-intensity factor was utilized, as expressed by

$$K = S\sqrt{\pi c}\ Y \quad , \tag{2}$$

where $Y = \sqrt{\sec \pi c/W}$ is the finite width correction, W being specimen width.

It should be noted that in some instance of surface flaw analysis, an additional magnification factor, termed M_K, is incorporated in Expression (1) to account for the stress magnification effects that may arise as the surface flaw approaches the back (or second) surface of a specimen. However, in the data analysis of this program, this factor has been omitted for two reasons: (1) the analytical formulation of M_K is somewhat controversial and (2) the companion programs on this recovery effort have omitted it. Furthermore, since most of the critical flaw sizes in this program have a depth-to-thickness ratio, a/t, of approximately two-thirds, the associated magnification factor would tend to increase the K values computed herein by 25 or 30 percent. This additional factor only serves to increase the disparities which were apparent between the reference K_{Ic} values and the terminal toughness values (see Table V) indicated in the spectrum tests. It was beyond the scope of this program to investigate this phenomenon further.

Crack Growth Measurement

Fatigue-crack propagation rates are determined from incremental measurements of the crack size as it advances under the applied cyclic loading. Where the fatigue-crack front extends entirely through the thickness of a test specimen, crack growth can be determined (approximately) during the test by measuring the crack growth on both surfaces. After fracture, these measurements can be corrected for the crack front curvature or "tunneling" which may be observed on the as-fractured surface.

In the case of surface or part-through cracks (which by definition do not penetrate the specimen thickness), only the crack growth along the specimen surface can be measured directly. The extent and rate of crack advance or penetration into the thickness cannot be observed visually during the test and can be determined only after fracture by measuring fatigue surface markings. Since the advance of the surface crack front is not always uniform, and since surface crack markings or "growth rings" may be either obliterated by environmental effects of indistinguishable in fatigue surface texture, an after-the-fact evaluation of crack growth is generally

less than satisfying for studying surface flaw behavior. It would be far more desirable, as well as more useful from a practical perspective, to be able to have a direct indication of surface crack enlargement. To that end, a crack-opening-compliance technique of monitoring crack extension has been utilized in this experimental program.

Compliance Measurement of Surface Crack Growth

The use of specimen compliance as a means of detecting and monitoring crack extension has been a common practice in fracture testing for a number of years. The common procedures are usually attributed to Boyle[(4)] and are based on the assumption of elastic behavior at the crack tip. In essence, the displacement equations of elastic-fracture mechanics are evaluated under the applied load conditions to determine the specimen displacements remote to the crack tip. By appropriate calibration, these displacement relationships can then be used to determine the flaw size under specified load conditions.

The actual displacements in cracked elastic body are influenced by both the overall structural geometry (i.e., specimen width) and by the local crack geometry (i.e., crack size and shape). Theoretically, displacement measurements at any point on a structure can provide information on crack size and crack extension. From a practical perspective, however, such displacement measurements are more sensitive to crack behavior as they approach the crack tip. Of course, there is also a finite measuring limit as the crack tip is approached.

Since cracks in experimental studies are usually generated from small mechanically created notches, it is convenient to instrument the mouth of the crack-starter notch with a strain gage or miniaturized clip gage to monitor the opening displacement of the notch. This procedure has become known as the crack-opening-displacement (COD)* technique of monitoring specimen compliance. If the notch is small and compact, its surface can be considered part of the crack surface such that the associated displacements can be related directly to analytical models of crack behavior. The importance of these measurements is not so much in their absolute values as it is in their relative value of reflecting crack size and extension.

---

* The term "crack opening displacement" is ambiguous. In this context, it should not be confused with the hypothetical stretch or deformation at the crack tip as proposed by Wells[(5)] for a fracture characterization, although one may be related to the other by certain mechanical inferences.

Displacements of the crack surfaces have been determined for the center-through crack by Westergard[6] and for the embedded flat elliptical crack by Green and Sneddon[7]. Although both of these analyses presume containment in an elastic body of infinite extent, the relationships are usually considered valid as long as the specimen is large in comparison with the crack size.

At the center or origin of the crack, the total COD (i.e., twice the surface displacement as measured from the reference coordinates) is, for the center through crack,

$$\mathrm{COD} = 2\varkappa_o = \frac{4(1 - \mu^2)Sc}{E} \quad , \tag{3}$$

and, for the flat elliptical crack,

$$\mathrm{COD} = 2\varkappa_o = \frac{4(1 - \mu^2)Sa}{E\Phi} \quad . \tag{4}$$

These expressions indicate that stress, crack size, and crack shape are the dominant factors influencing the COD, and that a calibration relationship of the general form

$$\mathrm{COD} = C\,\frac{Sa}{\Phi} \tag{5}$$

can be established for the surface flaw to correlate measured COD with actual crack size.

Calibration of Specimen Compliance

On most of the specimens, some reference fatigue-crack markings were available to establish a consistent elastic calibration between specimen compliance and crack size. These markings may have been bands of lower stress cycling intentionally inserted to identify the current state of flaw size, or they may have been the repetitive patterns of fatigue striations due to spectrum load. In either case, it was possible to select and measure three or more distinctive surface markings and associate them with the COD record. Then, by using Expression (3), a calibration scale factor was determined as

$$A = \frac{(\mathrm{COD})\ \Phi}{S \cdot a} \quad . \tag{6}$$

From this calibration, continuous output records of COD can be converted to crack growth records by the relation

$$a = \frac{(\mathrm{COD})\ \Phi}{A \cdot S} \quad . \tag{7}$$

It is this techniuqe which was used to determine the reference constant amplitude fatigue-crack propagation rates.

IV. – EXPERIMENTAL RESULTS

The principal experimental results of the three basic tasks contained in this program are presented in this portion of the report. The detailed data and other pertinent technical information are presented in referenced appendices.

Constant Amplitude Fatigue-Crack Propagation

The first task associated with providing an independent and supplementary evaluation of fatigue-crack propagation in D6AC steel plate was to ascertain that the materials and test procedures did indeed produce baseline results comparable with those derived by other investigators. To this end, baseline fatigue-crack propagation data were obtained from constant amplitude cyclic loading tests. Three tests at maximum cyclic stresses of 40, 60, and 100 ksi were conducted on 0.6-inch-thick specimens. One test at a maximum cyclic stress of 40 ksi was conducted on a 0.28-inch-thick specimen for comparison of thickness effects. All tests were run at a stress ratio, R, of 0.1 in a desiccated air environment. The rate results of these tests are presented in Figure 4. Superimposed on this figure, for purposes of comparison, is the reference scatterband of dry air fatigue-crack propagation data from the multilaboratory data compilation.[1]

It can be seen that the rate data derived from the constant-amplitude cyclic tests of this program are consistent between specimens, but fall below the reference band for compact-tension specimens of the multilaboratory program. Part of this deviation may be the result of the high (100 ksi) maximum cyclic stress imposed. These limited observations tend to support the maximum stress level effect suggested by Masters and White[8] No particular thickness or frequency effects are noted in the thinner specimen results.

From this task, it is concluded that the rate data are closely reproducible. However, some possible stress level effects remain which cannot be fully resolved at this time.

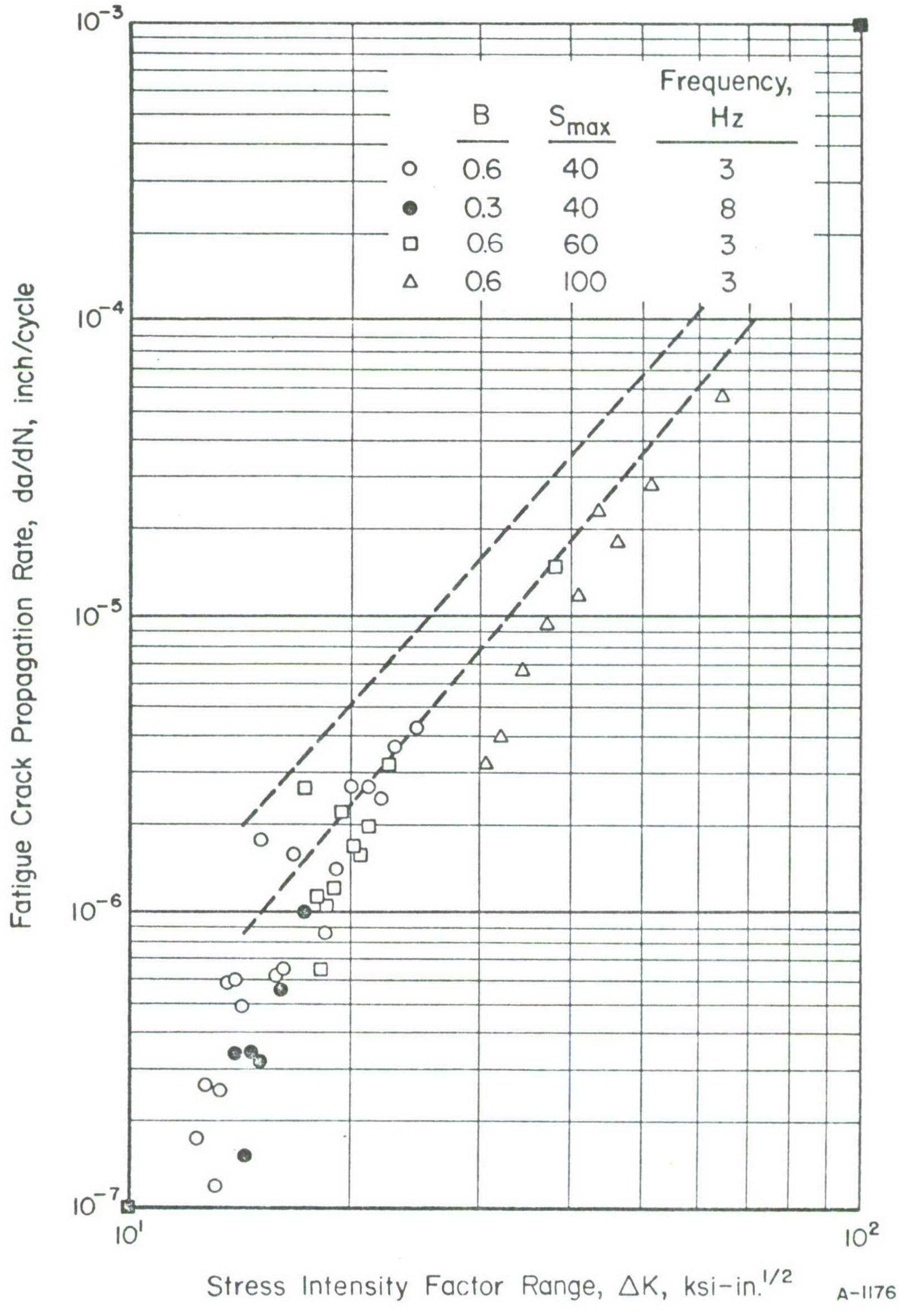

FIGURE 4. CONSTANT AMPLITUDE FATIGUE CRACK PROPAGATION RATES IN DESICCATED AIR FOR SURFACE FLAWS IN D6AC PLATE

Fatigue-Crack Propagation Under Simulated Flight Loadings

The second portion of this experimental program was concerned with the determination of fatigue-crack behavior under specific flight-loading spectra. The objective was to compare relative spectra severity and their interaction with environment. Eight specimens were used to evaluate five spectrum profiles in desiccated air and water-saturated JP-4 aircraft fuel environments. The particular loading spectra utilized in this program are listed in Table I and detailed in Appendix A. The general results of these tests are summarized in Table V. The test conditions, specimen size, initial and final flaw sizes, and the failure conditions are tabulated in this table.

If all specimens were uniform in fracture-toughness level and if all initial fatigue precracks were identical in size, the number of flight profiles applied to the specimens would be a direct measure of flight-load severity. However, such a consistent correlation was not evident. In fact, there was a discouraging disparity, especially with Specimen No. 6. As can be seen in Table V, as well as Table III, variations are evident both in the K_{Ic} level of this material and the size of the initial precracks. Thus, the fatigue-crack lifetime may vary as much from initial crack size and terminal conditions of toughness as from the actual severity of the loading spectrum.

Furthermore, as discussed in the Experimental Details section of this report, there appears to be an interaction between the initial precracking and subsequent variable-amplitude loading. Continuous monitoring of compliance frequently indicated that a large number of loading profiles were required to reestablish the stable continuous pattern of crack growth which had been initiated in precracking. Although a positive mechanism for this cannot be postulated, it is believed that this is a manifestation of the retardation associated merely with the precracking stress. As such, it is an unavoidable phenomenon whose behavior is dependent upon both the precracking stress and the distribution of the spectrum loads.

To eliminate some of these complexities and normalize the overall crack growth characteristics, an arbitrary crack size, from which continuous crack growth progressed, was selected as a reference benchmark. In these tests, a crack depth of 0.120 inch, or about twice the initial notch size, was selected. Crack lifetimes from this common point are summarized in Table VI. Load profile counts to three different crack sizes are presented in this table. First, growth in terms

Fatigue-Crack Propagation Under Simulated Flight Loadings

The second portion of this experimental program was concerned with the determination of fatigue-crack behavior under specific flight-loading spectra. The objective was to compare relative spectra severity and their interaction with environment. Eight specimens were used to evaluate five spectrum profiles in desiccated air and water-saturated JP-4 aircraft fuel environments. The particular loading spectra utilized in this program are listed in Table I and detailed in Appendix A. The general results of these tests are summarized in Table V. The test conditions, specimen size, initial and final flaw sizes, and the failure conditions are tabulated in this table.

If all specimens were uniform in fracture-toughness level and if all initial fatigue precracks were identical in size, the number of flight profiles applied to the specimens would be a direct measure of flight-load severity. However, such a consistent correlation was not evident. In fact, there was a discouraging disparity, especially with Specimen No. 6. As can be seen in Table V, as well as Table III, variations are evident both in the K_{Ic} level of this material and the size of the initial precracks. Thus, the fatigue-crack lifetime may vary as much from initial crack size and terminal conditions of toughness as from the actual severity of the loading spectrum.

Furthermore, as discussed in the Experimental Details section of this report, there appears to be an interaction between the initial precracking and subsequent variable-amplitude loading. Continuous monitoring of compliance frequently indicated that a large number of loading profiles were required to reestablish the stable continuous pattern of crack growth which had been initiated in precracking. Although a positive mechanism for this cannot be postulated, it is believed that this is a manifestation of the retardation associated merely with the precracking stress. As such, it is an unavoidable phenomenon whose behavior is dependent upon both the precracking stress and the distribution of the spectrum loads.

To eliminate some of these complexities and normalize the overall crack growth characteristics, an arbitrary crack size, from which continuous crack growth progressed, was selected as a reference benchmark. In these tests, a crack depth of 0.120 inch, or about twice the initial notch size, was selected. Crack lifetimes from this common point are summarized in Table VI. Load profile counts to three different crack sizes are presented in this table. First, growth in terms

TABLE V. SUMMARY OF FLIGHT LOAD SIMULATION TEST RESULTS

Specimen Number	Spectrum	Environment	Specimen Dimensions		Crack Measurements				Completed Profiles to Failure	Failure Stress, S_f, ksi	Maximum Stress in Spectrum, S_{max}, ksi	K at Failure[(a)]
					Initial		Final					
			Thick T	Width W	Depth a_i	Length $2c_i$	Depth a_f	Length $2c_f$				
3	5g MAC	Desiccated Air	.605	6.01	.080	.126	.405	.738	60	103.7	106.6	79
6	5g MAC	Water Saturated JP-4	.608	6.01	.089	.150	.489	.926	99	105.6	106.6	90
9	5g MAC w/Comp.	Water Saturated JP-4	.602	6.01	.088	.167	.370	.686	40	107.3	108.4	79
4	7.33g MAC	Desiccated Air	.590	6.01	.094	.190	.452	.872	46	105.8	106.7	88
8	7.33g MAC	Water Saturated JP-4	.602	5.99	.078	.140	.427	.725	57	106.3	106.7	84
10	5g CTB	Water Saturated JP-4	.598	6.01	.082	.146	.528	1.064	58	107.6	113.8	98
11	3g FB	Desiccated Air	.284	6.01	.080	.160	(b)	2.80	129[(d)]	62.1	66.4	151
12	3g FB	Water Saturated JP-4	.284	6.01	(c)	--	--	3.02	186[(d)]	65.7	66.4	171

(a) Calculated by Expression (1) or (2).

(b) Surface crack broke through back surface to develop full through-crack.

(c) Surface obliterated.

(d) Equivalent flight hours different than proceeding profiles. See Table 4.

of both profiles and equivalent flight hours (as specified by Table IV) are presented to a crack depth of 0.28 inch, which is breakthrough in the thin plate. Then, growth times are presented to breakthrough in the thick plate, or equivalently a crack length, 2c, of about 1.50 inches (for a typical aspect ratio of $a/2c \approx 0.4$). Finally, the actual failure time count is presented.

Within Table IV, only slight differences were noted between the desiccated air and water-saturated JP-4 environments for the frequencies considered in each spectrum condition. Of more importance are the dramatically shorter crack lifetimes (in terms of flight hours) associated with the lowest stress spectrum (3g FB). This is attributed to the lack of the higher beneficial peak loads which are characteristic of higher stress spectra.

To obtain an even more objective appraisal of spectrum severity, an evaluation of the gross crack-propagation rates in terms of profile increments has been included in this portion of the program. It is believed that this provides a more quantitative basis for comparing spectra severity and environmental effects.

In the following sections, a general description of the flight-load simulation tests is provided. Photomacrographs of the striation patterns which developed during propagation of the fatigue crack are shown as they appeared on the fracture surfaces. A tabulation of the striation measurements derived from these photomacrographs and the plotted crack growth curves are presented in Appendix B. Subsequently, the rate analysis based on striation pattern measurement and loading profiles is presented.

5g MAC Spectrum

Two tests, one in desiccated air (Specimen No. 3) and one in water-saturated JP-4 aircraft fuel (Specimen No. 6), were conducted with this flight-loading spectrum. Photomacrographs of each crack surface after failure are presented in Figures 5 and 6. A number of interesting features can be observed.

The patterns differ only in test environment; the former being for desiccated air, and the latter being for water-saturated JP-4 aircraft fuel. For all practical purposes, the striation or "growth ring" patterns are nearly identical in both of these specimens. The light areas represent the satin-like smooth texture of crack propagation under relatively low stress fatigue. The periodically

TABLE VI. SUMMARY OF CRACK LIFETIMES FROM A REFERENCE CRACK SIZE

						From Reference 0.120-inch Crack Depth To:					
						a = 0.28 inch		a = 0.60-inch or 2c ≈ 1.50 inch		Failure	
Specimen Number	Thickness B inch	Flight Spectrum	Environment	Profiles to Failure	Profiles to Develop Reference 0.120-inch Crack Depth	No. of Flight Profiles	Equiv. Flight Hours	No. of Flight Profiles	Equiv. Flight Hours	No. of Flight Profiles	Equiv. Flight Hours
3	.605	5g MAC	Desiccated Air	60	24	25	5000	--	--[a]	36	7200
6	.608	5g MAC	Water Saturated JP-4	99	63	24	4800	--	--	36	7200
9	.602	5g MAC w/comp.	Water Saturated JP-4	40	2	32	6400	--	--	38	7600
4	.590	7.33g MAC	Desiccated Air	46	5	30	6000	--	--	40	8000
8	.602	7.33g MAC	Water Saturated JP-4	57	16	32	6400	--	--	41	8200
10	.598	5g CTB	Water Saturated JP-4	58	14	31	6200	--	--	44	8800
11	.284	3g FB	Desiccated Air	129	20	90	472	104	546	109	573
12	.284	3g FB	Water Saturated JP-4	186	90	76	399	91	477	96	504

(a) Failure occurred before breakthrough in the thicker specimens.

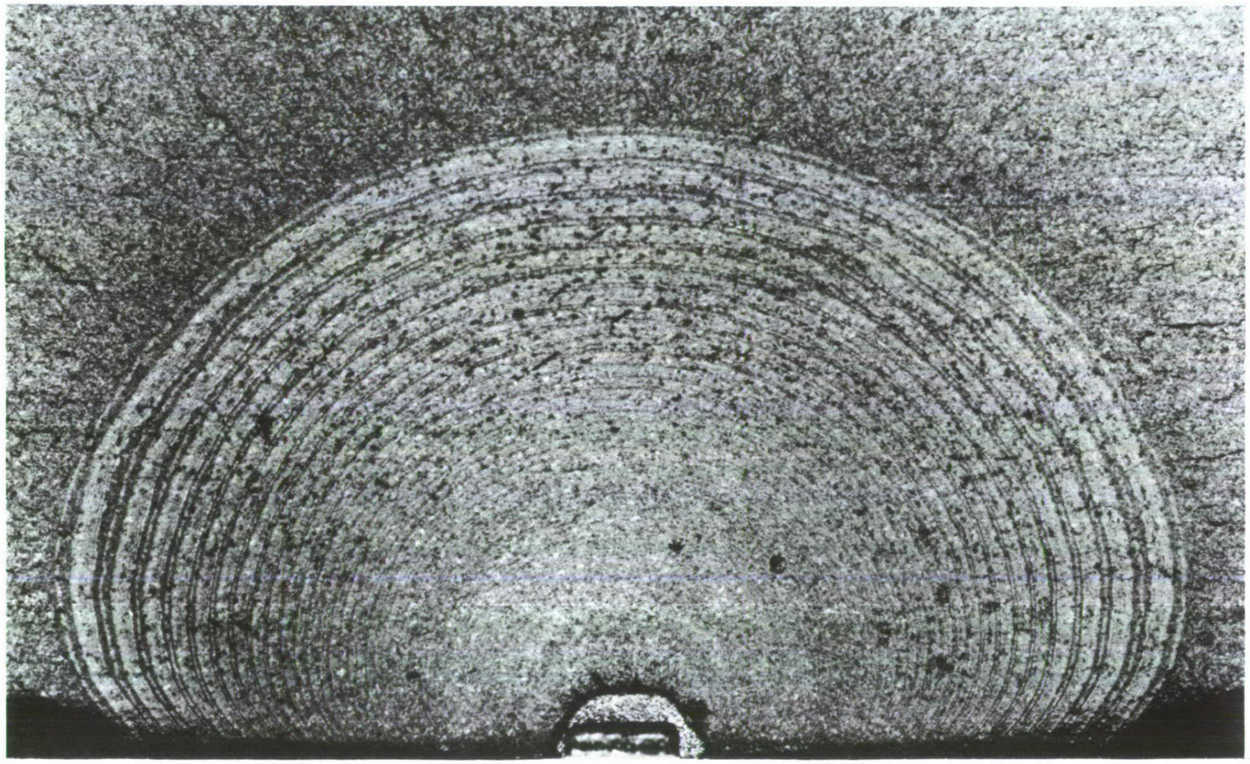

8X 5F263

FIGURE 5. STRIATION PATTERN OF SURFACE CRACK PROPAGATING IN SPECIMEN 3 UNDER 5-G MAC FLIGHT LOAD SPECTRUM IN DESICCATED AIR

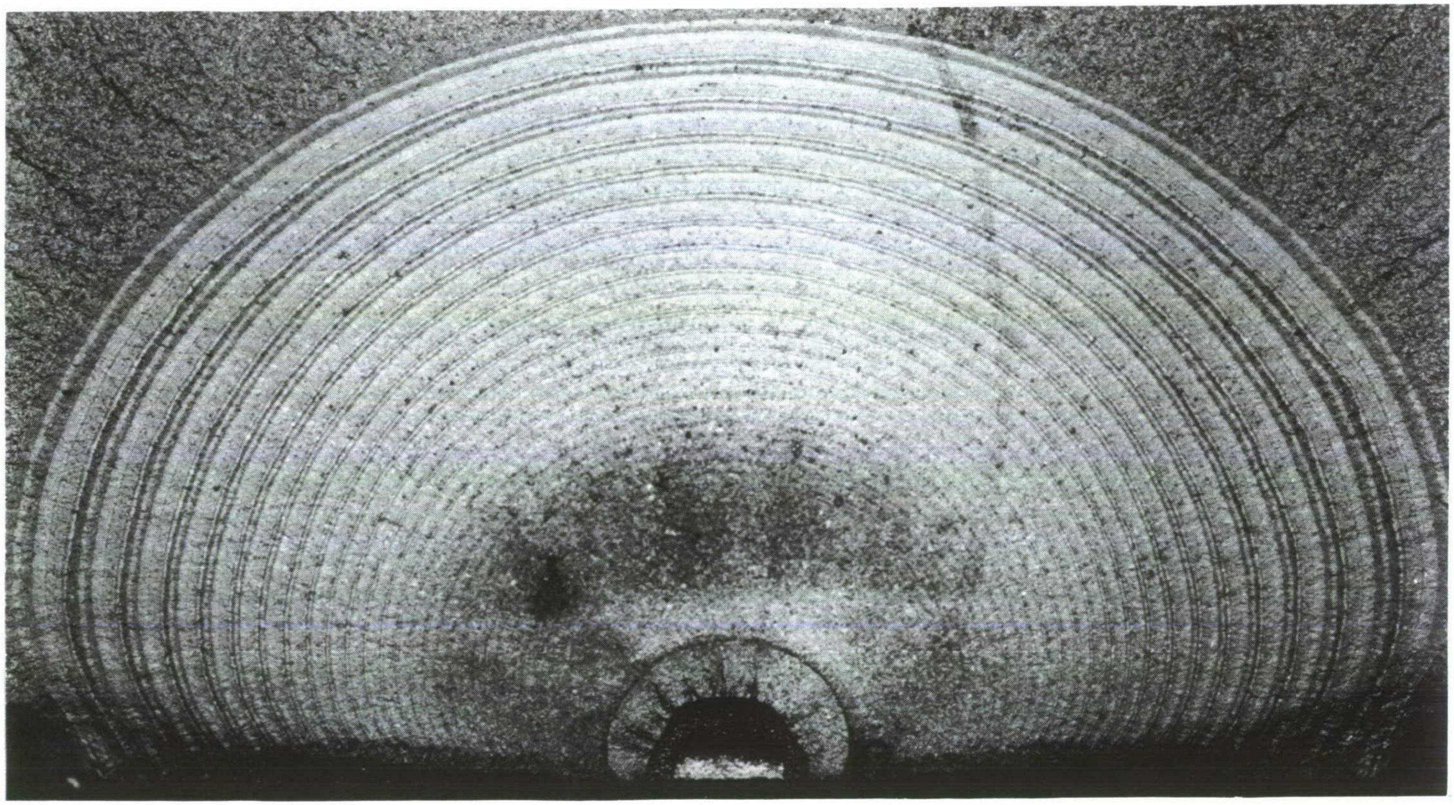

8X 5F716

FIGURE 6. STRIATION PATTERN OF SURFACE CRACK PROPAGATING IN SPECIMEN 6 UNDER 5-G MAC FLIGHT LOAD SPECTRUM IN WATER-SATURATED JP-4 AIRCRAFT FUEL

spaced darker bands represent the coarser textured surface due to the tearing action of a few interspersed high stress cycles. In particular, repeating pairs of dark bands are very dominant throughout the striation pattern. These are, respectively, the tenth and fifteenth layer high loads (reference Appendix A), the latter of which eventually drives the crack to a critical instability.

At this cyclic frequency, little difference is noted in the cyclic life of the test specimens as determined from a common initial crack size. Thus, the influence of water-saturated fuel environment is considered negligible at this cyclic frequency. Also, no particular corrosive degradation of the striation pattern is evident due to this fuel environment.

5g MAC Spectrum with Compression

To evaluate the influence of compressive load cycles on spectrum behavior, the previous 5g MAC spectrum was augmented[9] by the Air Force Flight Dynamics Laboratory to include some negative load occurrences and an additional positive peak. One test with Specimen 9 in water-saturated JP-4 was conducted with this spectrum.

Some significant variations can be noted in the photomacrograph presented in Figure 7. The repeating doublet pattern noted in Figures 5 and 6 now appears as four or five darker bands occurring with more regularity on the lighter (more satin-like) fatigue surface. This is attributed to the larger cluster of high loads (four or five), one of which (layer 32) is also associated with the extreme negative load excursion. A slight increase in crack lifetime can be noted in Table VI.

7.33g MAC Spectrum

The influence of this flight-load spectrum was evaluated with one test (Specimen 4) in desiccated air and one test (Specimen 8) in water-saturated JP-4 aircraft fuel. The resulting striation patterns are shown in Figures 8 and 9. The apparent reversal in environmental influence, which may be noted in Table VI, is attributed to scatter in material behavior with negligible environmental influences.

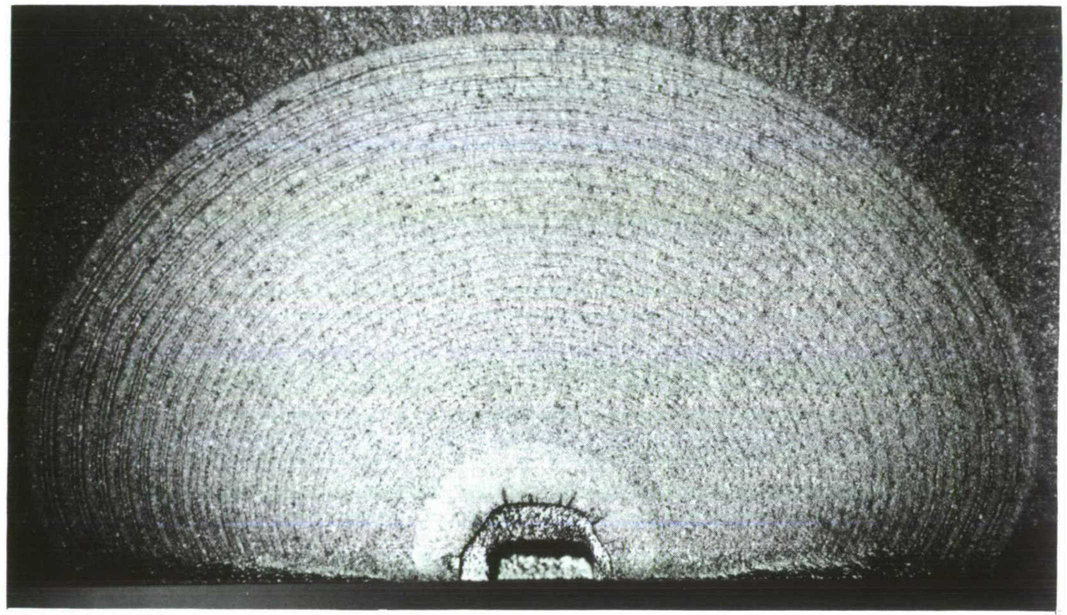

8X 5F825

FIGURE 7. STRIATION PATTERN OF SURFACE CRACK PROPAGATING IN SPECIMEN 9 UNDER 5-G MAC FLIGHT LOAD SPECTRUM WITH COMPRESSION LOADS IN WATER-SATURATED JP-4 AIRCRAFT FUEL

Although this spectrum has a more detailed layering of loads, it does not appear significantly more severe in the average intensity and occurrence of loads. In fact, from Appendix A tabulation, the distribution of peak loads appears to be somewhat more uniform. Accordingly, in the striation patterns of Figures 8 and 9, the darker tear bands are not as tightly clustered as in the previous spectra.

5g CTB Spectrum

Specimen No. 10 was used to evaluate this spectrum in water-saturated JP-4 aircraft fuel. This spectrum had the highest load excursion of the five spectra considered in this program, yet it had the longest flight-hour lifetime to failure. Part of this is attributed to the beneficial retardation effect brought about by the peak loads, and part to the apparently high terminal toughness level of this particular specimen as indicated in Table V. The striation pattern illustrated in Figure 10 reveals the close clustering of peak load tearing which would be anticipated from the load distribution presented in Appendix A.

3g FB Spectrum

The thinner section (0.28 inch) specimens were used to evaluate this loading spectrum. Specimen 11 was tested in desiccated air; Specimen 12 was tested in water-saturated JP-4 fuel. The thinness and toughness level of these specimens permitted breakthrough of the surface flaw and extension growth of the crack in the center-crack configuration. The striation patterns of these fracture surfaces are shown in Figures 11 and 12. The surface flaw growth phase of Specimen 12 was obliterated by environmental effects and could not be measured.

Rate Analysis of Flight-Loading Spectra

Several attempts have been made to predict actual crack growth curves with several of the crack-life integration routines in an effort to evaluate spectrum severity. These computational procedures were very sensitive to both the flaw size initially assumed and the terminal material toughness, as well as to the particular retardation factor. The results of attempting to match measured crack growth curves to those which were analytically generated were less than satisfactory. Only slight variations in the basic fatigue-crack propagation rate constants, such as are frequently encountered experimentally, caused major deviations in the resultant

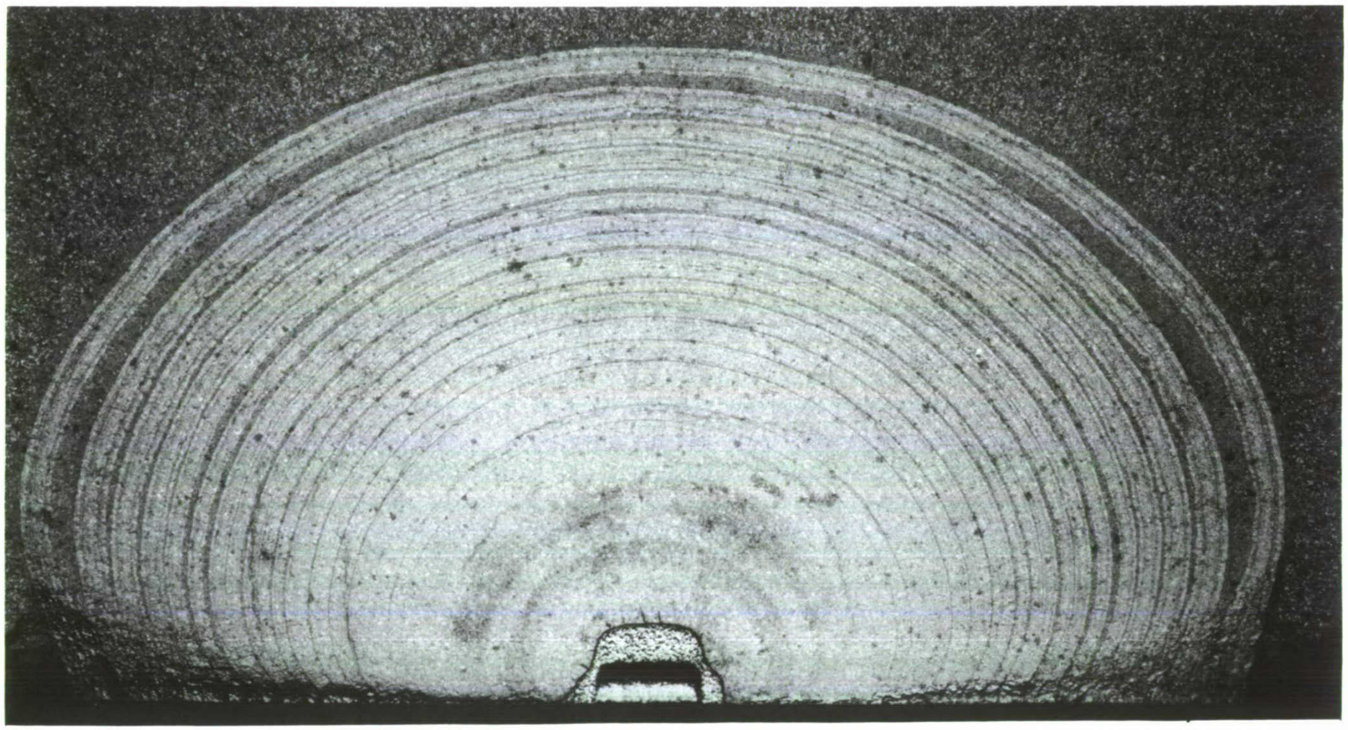

8X 5F712

FIGURE 8. STRIATION PATTERN FOR SURFACE CRACK PROPAGATING IN SPECIMEN 4 UNDER 7.33-G MAC FLIGHT LOAD SPECTRUM IN DESICCATED AIR

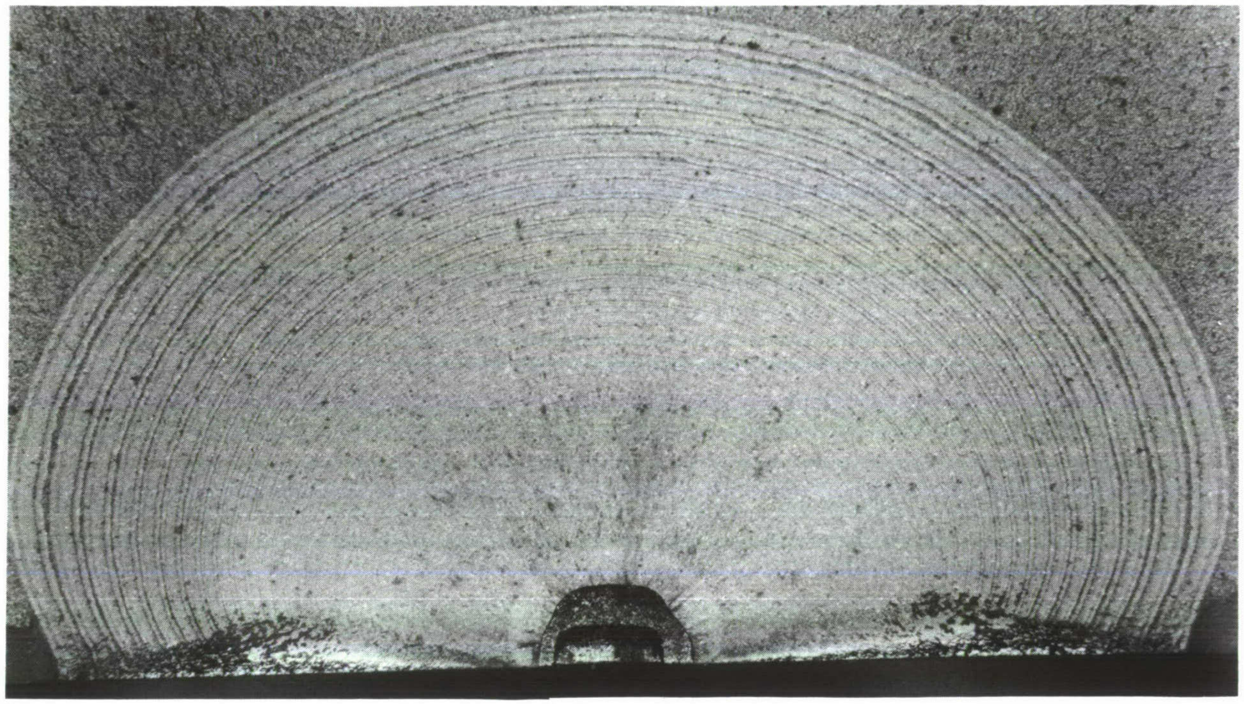

8X 5F755

FIGURE 9. STRIATION PATTERN FOR SURFACE CRACK PROPAGATING IN SPECIMEN 8 UNDER 7.33-G MAC FLIGHT LOAD SPECTRUM IN WATER-SATURATED JP-4 AIRCRAFT FUEL

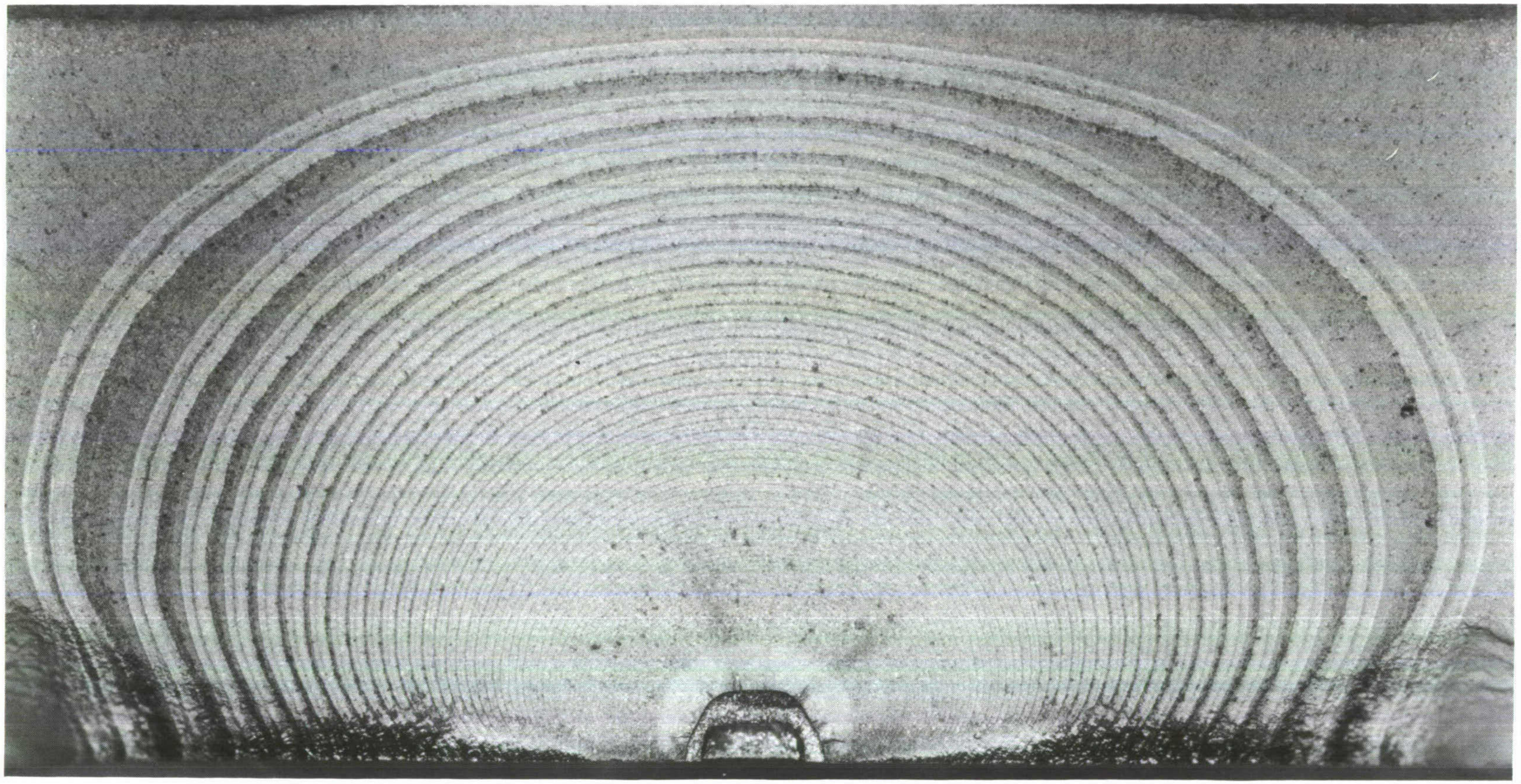

8X 5F906

FIGURE 10. STRIATION PATTERN FOR SURFACE CRACK PROPAGATING IN SPECIMEN 10 UNDER 5-G CTB FLIGHT LOAD SPECTRUM IN WATER-SATURATED JP-4 AIRCRAFT FUEL

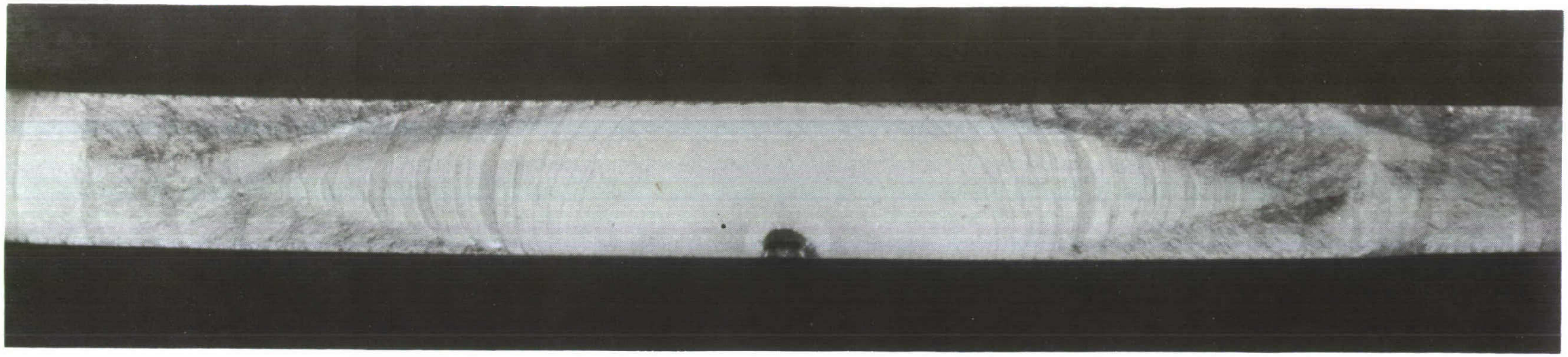

3X 6F364

FIGURE 11. STRIATION PATTERN FOR SURFACE CRACK PROPAGATING IN SPECIMEN 11 UNDER 3-G FB FLIGHT LOAD SPECTRUM IN DESICCATED AIR

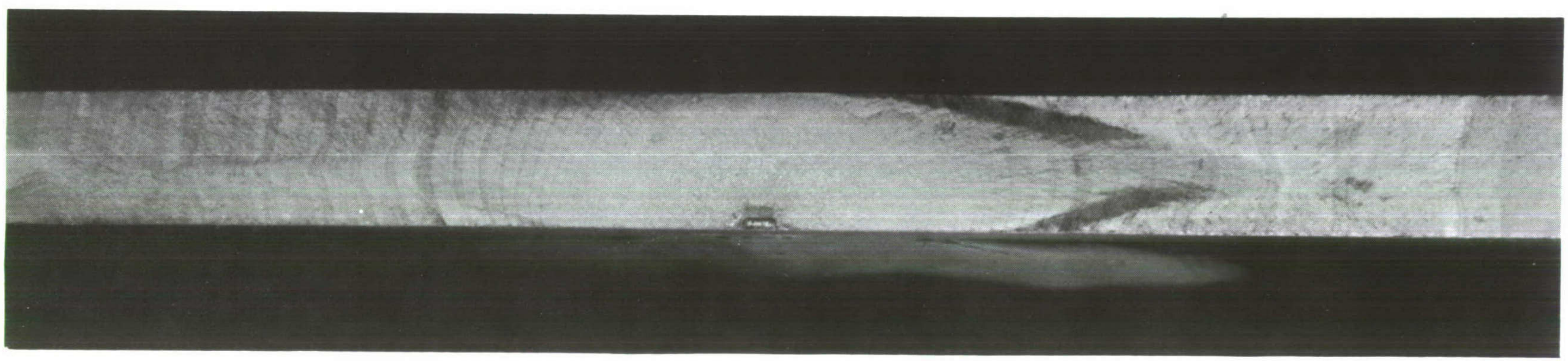

3X 6F367

FIGURE 12. STRIATION PATTERN FOR SURFACE CRACK PROPAGATING IN SPECIMEN 12 UNDER 3-G FB FLIGHT LOAD SPECTRUM IN WATER-SATURATED JP-4 AIRCRAFT FUEL

retardation factors such that these factors did not reveal a direct correlation of behavior. Finally a rate analysis approach was adopted.

The crack growth rate analysis usually conducted on constant amplitude fatigue-crack propagation data has the form

$$da/dN = f(\Delta K) \quad , \tag{8}$$

where a = crack size

N = number of cycles

ΔK = stress-intensity factor range.

In analogy to this, a crack growth rate analysis based on the number of repetitive profiles can be conducted on variable amplitude fatigue-crack propagation data. Although there is no particular precedent for doing this, the smooth regularity of the crack growth curve forms shown in Figures B-1 through B-6 of Appendix B and developed from the preceding striation patterns suggest that such a rate model may be useful.

To develop this, the number of repetitive profiles, N_p, is used as the differentiating variable, and ΔK_p is based simply on the zero-to-maximum stress range* of the complete profile. The resulting rate model is

$$da/dN_p = f(\Delta K_p) \quad . \tag{9}$$

The data previously cited have been analyzed by this procedure and are graphically displayed in Figures 13, 14, and 15.

Of the 5g spectra presented in Figure 13, it appears that the 5g MAC spectrum in water-saturated JP-4 aircraft fuel is the more severe environment. The 5g MAC spectrum with compression and 5g CTB spectrum following in that order of severity for the water-saturated JP-4 aircraft fuel environment. At high ΔK values, these spectra (along with the dry air 5g MAC spectrum) appear to converge, indicating that the fatigue process per se dominates over environment at these higher stress-intensity factor levels.

The 7.33g MAC spectrum presented in Figure 14 indicates slightly less environmental influence due to water-saturated JP-4 aircraft fuel than was noted in the 5g spectra. Generally, however, very little difference is noted between the two sets of spectra shown in these figures on a rate basis.

---

* Since the minimum stress of these profiles is zero or less (i.e., negative), and since a strong effect of negative load excursion was not noted, the simplistic approach of assuming $\Delta K = K_{max}$ has been adopted here.

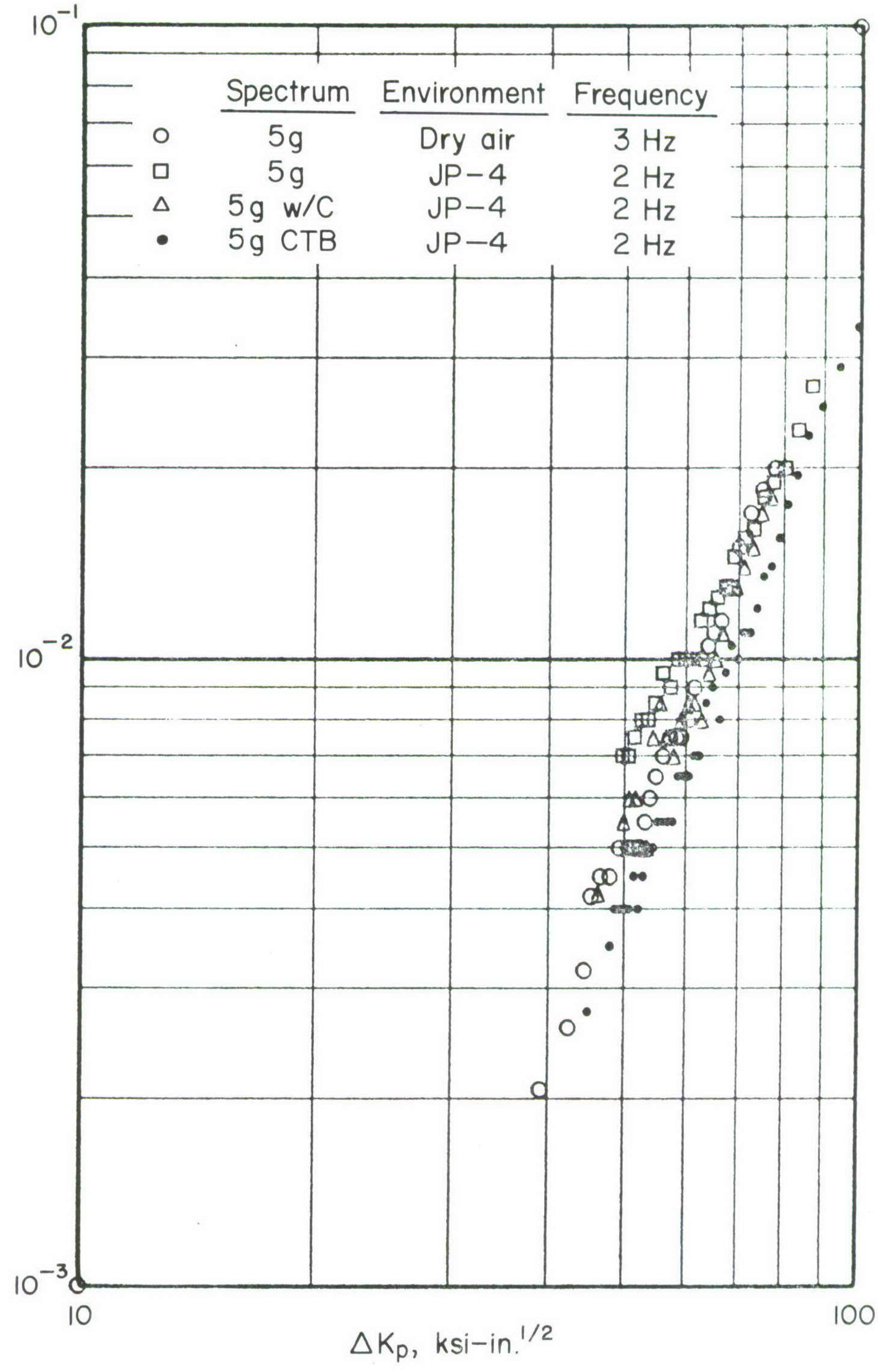

FIGURE 13. PROFILE GROWTH RATES IN VARIOUS 5g SPECTRA (200 FLIGHT HOURS PER PROFILE)

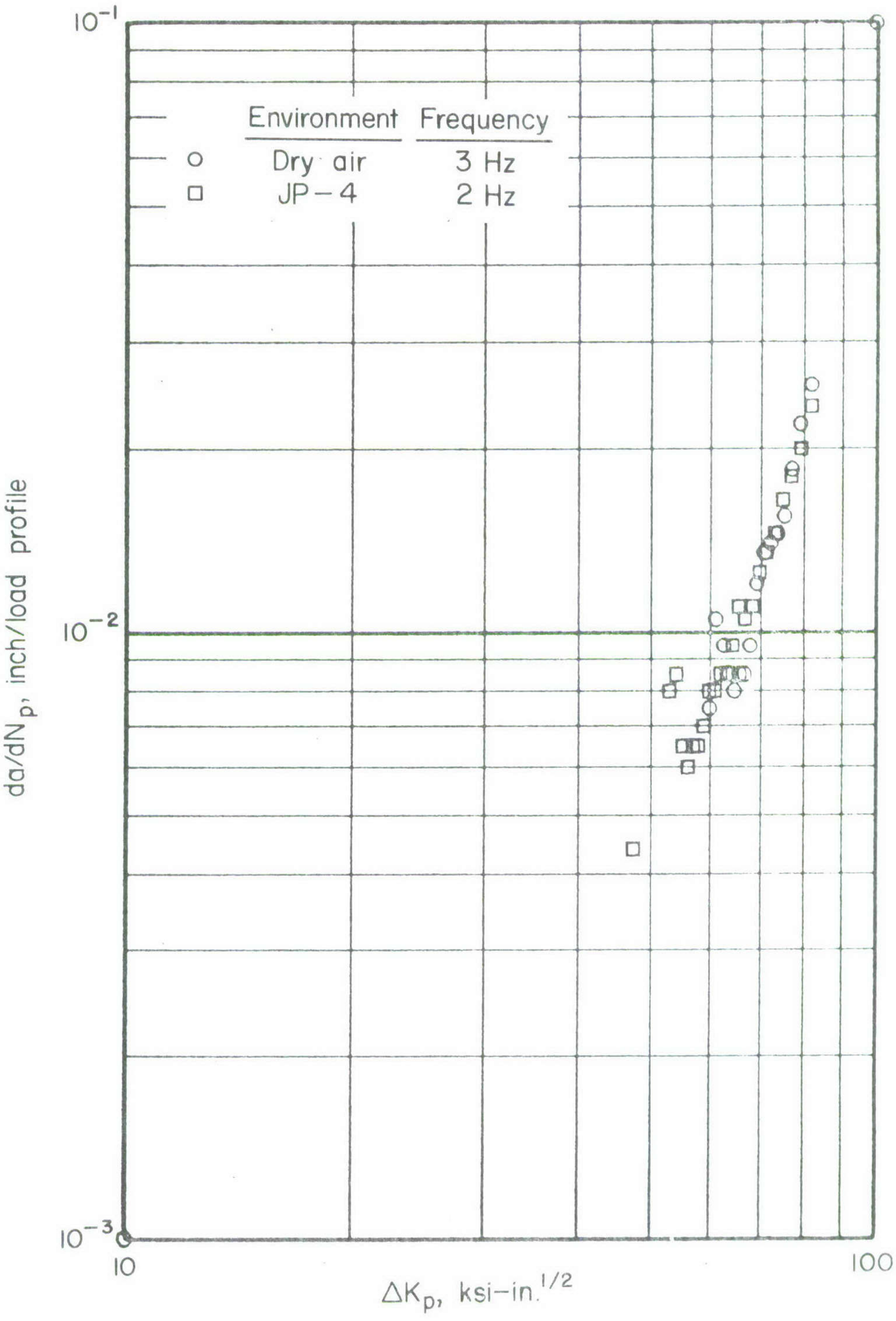

FIGURE 14. PROFILE GROWTH RATES IN THE 7.33g MAC SPECTRA (200 FLIGHT HOURS PER PROFILE)

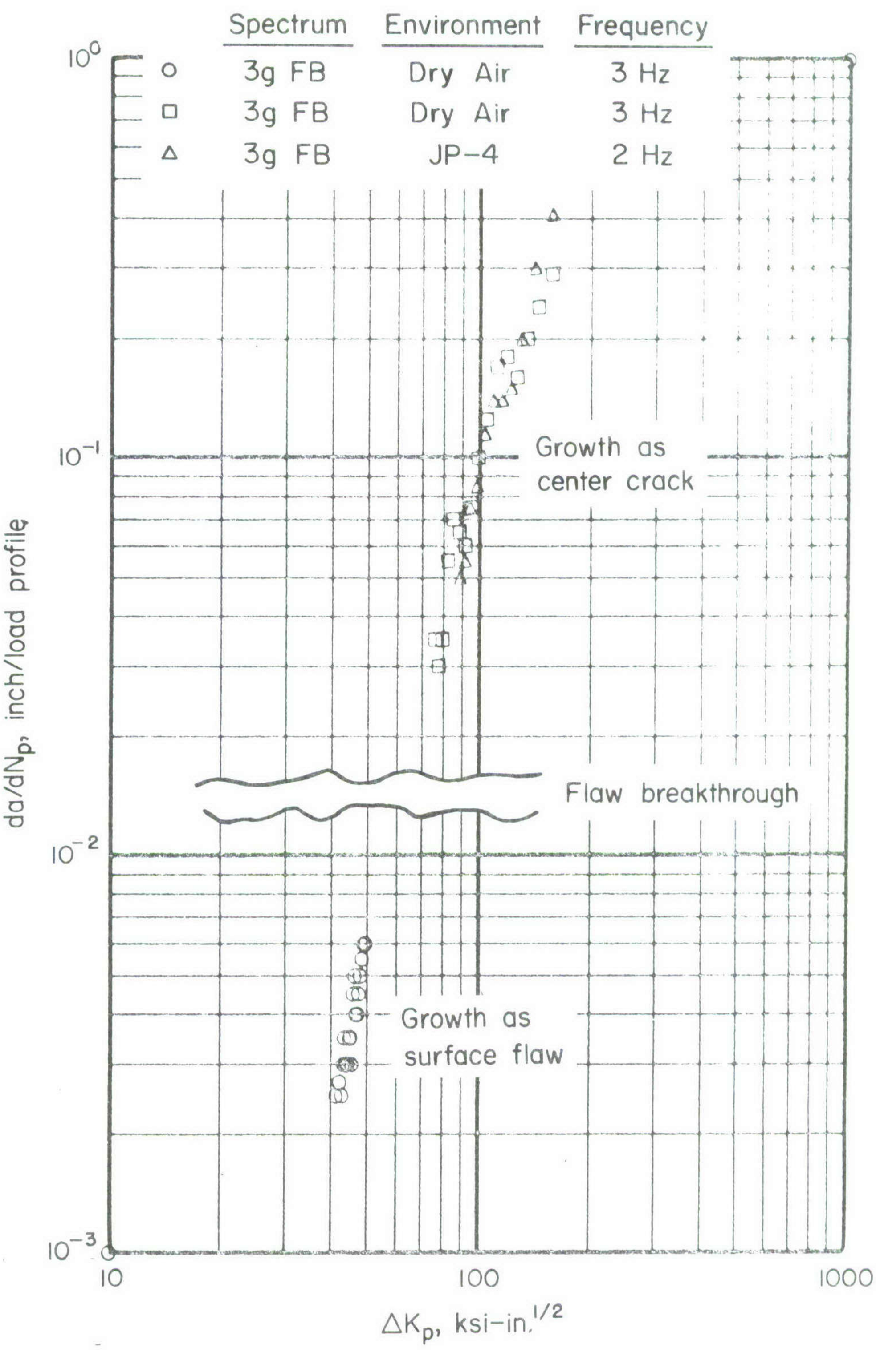

FIGURE 15. PROFILE GROWTH RATES IN THE 3g FB SPECTRUM (5.25 FLIGHT HOURS PER PROFILE)

Figures 13 and 14 can be compared with each other directly since they represent the same number of flight hours per load profile. However, Figure 15 must be considered separately since it represents a smaller number of flight hours per load profile as indicated in Table IV. Although these data could also be normalized on a flight time basis, it is considered more important to emphasize the profile characteristics per se.

The 3g FB spectrum rate data presented in Figure 15 illustrate the effects of flaw breakthrough or transition to the center-crack configuration. It is interesting to note that a continuity in the rate trend is apparent, although the precise nature of the transition could not be identified. Surface flaw rate data for the JP-4 aircraft fuel could not be determined because the striation pattern was obliterated.

One of the most striking features of these data displays is the quasi-linearity of the rate trend on these logarithmic coordinates. Such a linearity is very reminiscent of the Paris[10,11] model of basic constant amplitude fatigue-crack propagation; that is,

$$da/dN = C(\Delta K)^n \quad . \tag{10}$$

This may be surprising in view of the complex loading profiles which involve numerous stress ratios and retardation effects. That such simple behavior still prevails motivated a further look into crack-life integration routines.

Using the Air Force Computer Program "CRACKS"[12], a crack growth prediction was made for one initial crack size (a = .090 inch) using both the Paris and Forman[13] rate equations with several values of the Wheeler[14] retardation factor. The crack size and number of profiles information generated by this computer program were then analyzed in terms of crack growth rate. These results are summarized in Figure 16. The rate constants, while typical, are selected for illustration purposes only.

The linearity which was apparent experimentally is evident here also. This suggests that in spite of cycle load complexity, crack growth on the profile increment is a nearly linear process. Furthermore, the test specimen is an excellent integrating device in itself, as has been suggested by Broek[15].

By comparing the predictions of Figure 16 with the experimental results of Figure 13, it can be seen that the test results may be represented by the Forman equation with $m \approx 2.2$, or by the Paris equation with $m \approx 1.8$ for the particular C and n values which were used.

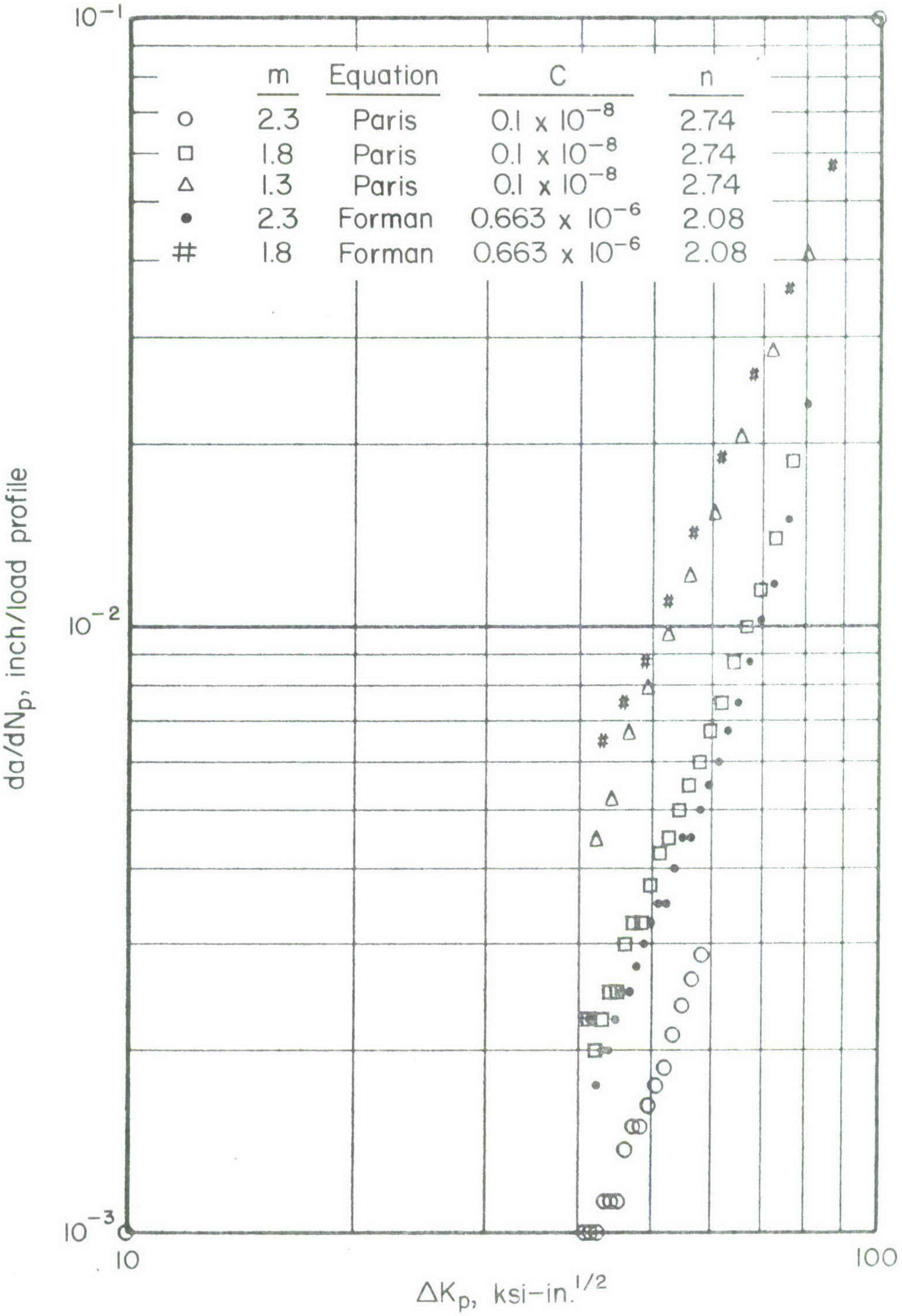

FIGURE 16. PROFILE GROWTH RATES PREDICTED BY PROGRAM CRACKS FOR THE 5g MAC SPECTRUM

From this exercise, it was concluded that spectrum severity can be evaluated best by a rate analysis technique. Although crack growth integration routines have a definite role in determining the absolute severity of specific damage situations, they are subject to significant variations when applied to general cases wherein the initial damage and terminal material toughness is not known precisely.

General Observations

From the preceding results, there are several general observations which can be made. It is evident that peak loads influence crack extension in two ways. During their application, a distinct tearing process is apparent. However, upon their release, they induce residual blunting or retardation effects to delay subsequent fatigue-crack growth at lower load levels. As a result, the net effective crack growth is dependent upon a trade-off between the amount of tearing and the amount of subsequent retardation which is caused. The distribution of the peak loads within the spectrum profile is also an important factor in the overall rate of cracking.

From the large differences in crack lifetimes that exist between the relatively high load spectra (5g and 7.33g) and the lower load spectrum (3g), it is apparent that the relationship of peak load level to tensile yield-strength level is very significant in the amount of retardation. This is consistent with the many observations which indicate that spectrum truncation decreases fatigue-crack lifetime.

A final observation of interest is the variation of the terminal toughness values presented in Table V. The first six specimens which failed in the surface flaw mode exhibit a range of K values comparable with the reference values of Table III. However, the last two specimens which finally failed in the center cracked mode exhibit a terminal toughness substantially above this level. While this is attributed primarily to the stress-state change attendant to the smaller thickness, it is also conceivable that fracture direction effects are influential in these values.

Retardation Studies

To verify some of the basic trends which have been observed in regard to fatigue-crack growth retardation in D6AC steel plate, a series of single overload tests were conducted. The objective of these tests was to determine the

number of constant amplitude cycles which would be retarded, dampened, or attenuated following an overload excursion which may "blunt" the crack tip through localized crack tip plastic deformation.

The test matrix for this portion of the program has been tabulated in Table I. Overload ratios selecting two positive and one negative level of load excursion were considered for the two thicknesses of D6AC plate. Maximum cyclic stress levels of 40, 60, and 80 ksi were used to provide a range of applied stress-intensity factor levels.

The details of this portion of the experimental program are discussed in the following subsections. First, the retardation phenomenon is discussed; then, the technique of evaluation is described. Finally, a summary of results is presented.

Retardation Effects in Fatigue-Crack Propagation

Load excursions above the nominal maximum cyclic stress level associated with a given constant amplitude cyclic loading may alter the effective crack propagation rates associated with that given by constant amplitude cyclic conditions. The overload may "blunt" and retard the advancing fatigue crack by enlarging the plastic enclave at the crack tip. Or, if the overload condition is sufficiently close to the critical fracture condition, crack growth may be accelerated by the stable tearing process which precedes fracture. In either case, the interaction of occasional overloads with a constant amplitude cyclic loading changes the propagation rate normally associated with constant amplitude process.

Of primary interest in this task was the retardation phenomenon. The plastic zone which progressed in a relatively uniform manner in constant amplitude fatigue may be expanded suddenly by a large load excursion. The resulting plastic enclave at the crack tip may act, for subsequent lower amplitude loadsing, as a compressively prestressed zone, retarding or delaying further crack advance.

On crack growth curves, where crack length is displayed as a function of cyclic count, this phenomenon is manifested as a plateau or step in the curves as illustrated in Figure 17. The number of cycles attenuated or retarded, N_r, at a given overload is arbitrarily defined as the number of cycles to reestablish the crack propagation rate existing immediately prior to the overload. The actual behavior of retardation is dependent upon the applied overload, the duration or number of cycles of overload, the shape of the plastic enclave, the stress-strain response of the material, and other mechanical details. Although this concept is largely qualitative, it is the basis for empirical models of given retardation effects.

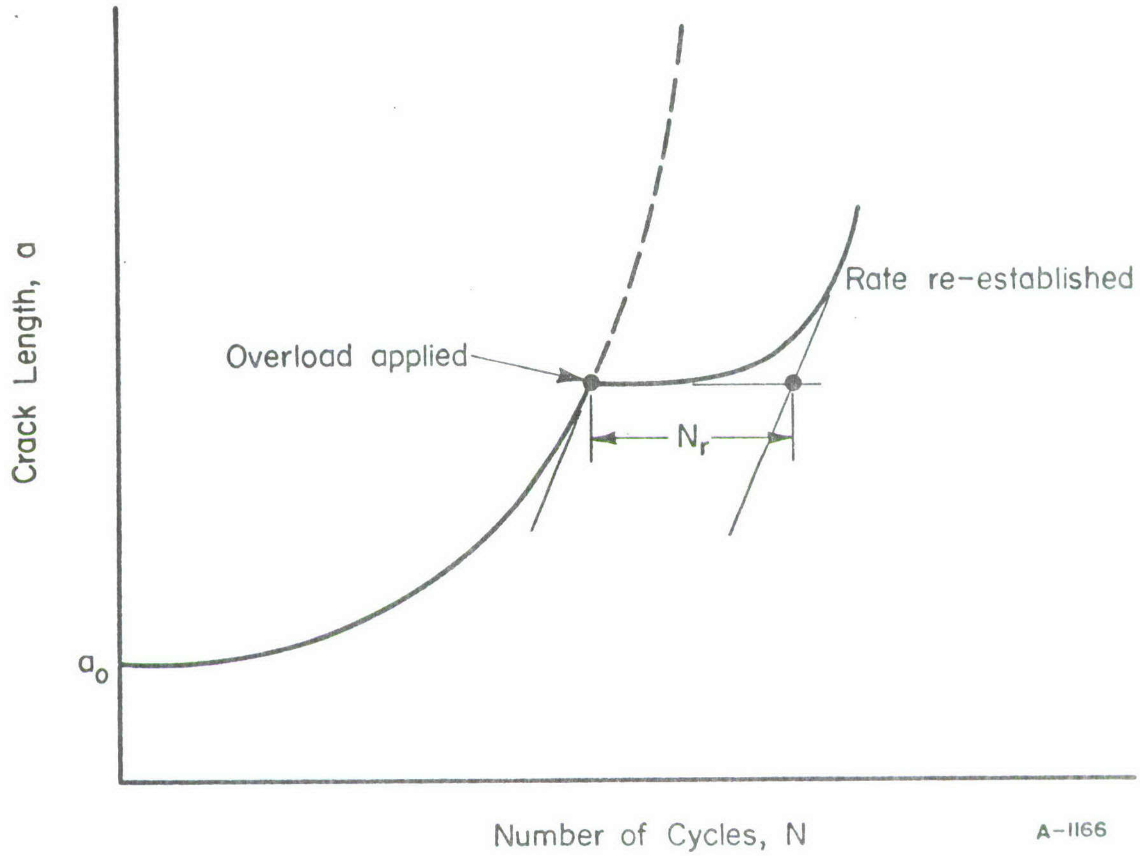

FIGURE 17. RETARDATION PHENOMENON ON THE CRACK GROWTH CURVE

Determination of Crack Growth Retardation

Crack growth retardation characteristics are evaluated by interrupting a constant amplitude fatigue crack propagation test with a single peak overload. The applied cyclic stress profile appears as shown in Figure 18. At the application of the overload stress, S_{peak}, the crack tip is blunted or plastically deformed such that at subsequent lower stress, constant amplitude cycling, crack growth is delayed as previously illustrated in Figure 17.

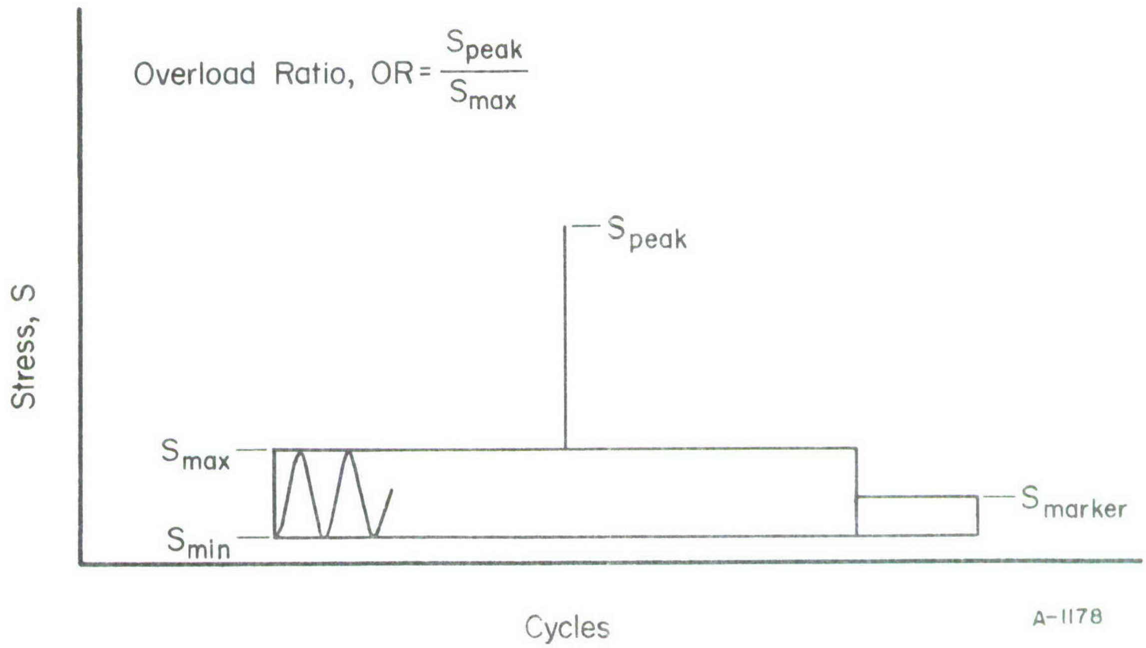

FIGURE 18. APPLIED CYCLIC STRESS PROFILES FOR RETARDATION STUDIES

Continuous compliance monitoring of crack growth permits a direct graphical measurement of the number of cycles retarded. This, in combination with the applied stresses, permits the calculation of the associated K_{peak} and K_{max} values at the point of overload.

Retardation Test Results

The principal results of the retardation tests are summarized in Figure 19. The number of cycles retarded or attenuated is displayed as a function of overload

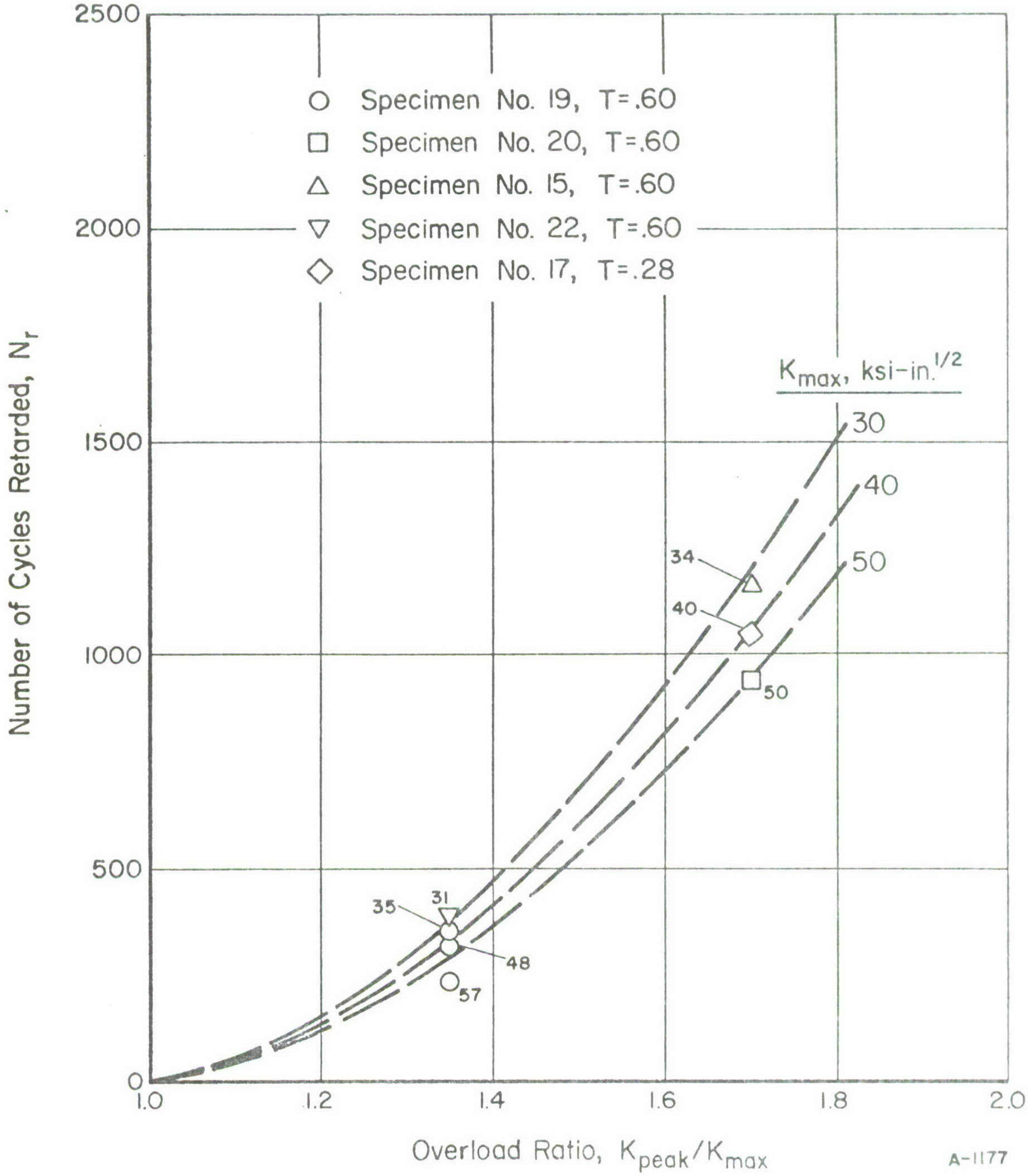

FIGURE 19. CRACK GROWTH RETARDATION DUE TO SINGLE OVERLOADS

ratio for several levels of maximum cyclic stress level. Symbols denote experimentally determined values; the dashed lines indicate the general relations graphically interpolated from these data.

It should be noted that in these tests no retardation was observed for the negative load excursions (i.e., OR = -0.35). Hence, no significant results can be indicated for Specimen Nos. 14, 16, and 21. Although the compression-augmented 5g MAC spectrum (Specimen No. 9) of the flight load simulation tests indicated that compression loads do contribute somewhat to crack growth retardation, it was not evident in these single overload tests. Possibly, the duration of repetition of these single peak loads was inadequate to reinforce this effect.

V. – CONCLUSIONS

The results of this experimental program confirm that occasional overload excursions with their resultant crack growth retardation are a postive mechanism for extending fatigue-crack lifetime beyond that which would be encountered in a constant-amplitude cyclic load condition. This implies that the linear cumulative damage hypothesis is indeed conservative when applied to situations of variable amplitude cyclic loadings.

Crack growth retardation was evident in all spectrum tests. Very regular behavior was noted when the spectra were evaluated as a rate process in terms of profile increments. When the rate data for the high load spectra (5g and 7.33g) are reduced to a cyclic basis, an average crack growth rate of about 0.6 microinches per cycle is noted in the mid-range of ΔK. This is at least an order of magnitude below the constant amplitude cyclic crack growth rates for equivalent levels of ΔK and is a very positive indication of retardation effects. In the lower load spectrum (3g), crack growth retardation, while evident, was not as pronounced.

In the flight load simulation tests of this program, it is seen that spectra with high peak loads (i.e., loading peaks in excess of one-half the tensile yield strength, such as the 5g MAC, 7.33g MAC, and 5g CTB spectra) sustain crack lifetimes an order of magnitude greater than spectra with low peak loads (i.e., loading peaks less than one-half of the tensile yield strength, such as the 3g FB spectrum).

At the cyclic frequencies of these tests, the environmental influence of the water-saturated JP-4 aircraft fuel presented only a very slight acceleration of the crack growth rates noted in dry air. While a large degree of environmental aggravation was not expected, a more pronounced difference would probably have been encountered at lower cyclic frequencies.

The analytical prediction of crack growth curves appears to be as heavily dependent upon initial flaw size as it does upon the selection of m, C, and n, the various growth rate parameters. Since, in general, the initial flaw size is very elusive to identify and quantify in absolute dimensional size, it may be more expedient to assess defect severity by a nondestructive testing indicator (or proof-test measure). Then, experimentally, a test specimen with a similar measure of severity could be used as the integrating device for flaw growth. That is, one might choose not to rely as much on the analytical prediction of flaw growth as that growth determined from an experimenal simulation of the flaw.

It does appear that improved crack growth prediction models can be developed. However, they will need to account for peak load tearing, as well as the peak-load-to-yield-strength relationship. Furthermore, it must be recognized that the retardation process is dependent upon the maximum K level, as well as the overload ratio of peak K to maximum K levels.

VI. - REFERENCES

1. Feddersen, C. E., Moon, D. P., and Hyler, W. S., "Crack Behavior in D6AC Steel", Metals and Ceramics Information Center Report MCIC-72-04, Battelle's Columbus Laboratories (January, 1972).

2. Irwin, G. R., "Crack Extension Force for a Part-Through Crack in a Plate", Journal of Applied Mechanics, 84, 4 (1962).

3. Irwin, G. R., "Analysis of Stresses and Strains Near the End of a Crack Transversing a Plate", Journal of Applied Mechanics, 24, 3 (1957), pp 361-364.

4. Boyle, R. W., "A Method for Determining Crack Growth in Notched Sheet Specimens", Materials Research and Standards, 2, (1962), pp 646-651.

5. Wells, A. A., "Unstable Crack Propagation in Metals", Procedures of the Crack Propagation Symposium, Cranfield (1962).

6. Westergaard, H. M., "Bearing Pressures and Cracks", Journal of Applied Mechanics, 61 (1939), pp A49-A53.

7. Green, A. E., and Sneddon, I. N., "The Distribution of Stress in the Neighborhood of a Flat Elliptical Crack in an Elastic Solid", Proceedings of the Cambridge Philosophical Society, Vol. 46 (1950), pp 159-163.

8. Masters, J. N., and White, J. L., "Development of Fracture Toughness Properties of D6AC Steel for F-111 Applications", AFML-TR-70-113, The Boeing Company (January, 1971).

9. Wood. H. A., AFFDL Spectrum Development, Meeting Passout (April 14, 1971).

10. Paris, P. C., Gomez, M. P., and Anderson, W. E., "A Rational Analytic Theory of Fatigue", Trends in Engineering (University of Washington), 13, 1 (1961).

11. Paris, P. C., "The Growth of Cracks Due to Variation in Load", Ph.D. Thesis, Lehigh University (1962).

12. Engle, R. M., Jr., "Cracks, A Fortran IV Digital Computer Program for Crack Propagation Analysis", AFFDL-TR-70-107, Air Force Flight Dynamics Laboratory (October, 1970).

13. Wheeler, O. E., "Crack Growth Under Spectrum Loading", Report No. FZM-5602, General Dynamics Corporation, Convair Aerospace Division (June, 1970).

14. Forman, R. C., Kearney, V. E., and Engle, R. M., "Numerical Analysis of Crack Propagation in Cyclic-Loaded Structures", J. Basic Engineering, Transactions, ASME, 89 (1967), pp 459-464.

15. Broek, D., "Concepts in Fail-Safe Design of Aircraft Structures", DMIC Memorandum 252, Battelle's Columbus Laboratories (March, 1971).

16. Little, C. A., and Bunting, P. M., "Crack Propagation Test Spectra", Report No. FZM-12-13269, General Dynamics Corporation, Convair Aerospace Division (April, 1971)

17. Newman, J. C., Communication from National Aeronautics and Space Administration, Langley Research Center, Hampton, Virginia.

APPENDIX A

SPECTRUM LOADING PROFILES

APPENDIX A

SPECTRUM LOADING PROFILES

The variable amplitude loading profiles which have been used in experimental program are tabulated in this appendix. Tables A-I and A-II present the basic 5g and 7.33g MAC spectra, respectively, as defined in Reference 16. Table A-III presents the 5g MAC spectrum as modified in Reference 9 to include compression loadings. This spectrum was selected to investigate the effect of compression loads on the overall crack growth rates. Table A-IV lists the 5g CTB (carry-through box) spectrum representing another structural location. This spectrum was described by Reference 16 and randomized in Reference 17. The particular profile of the latter source was adopted in this program so that correlation from another laboratory would be possible. Finally, the loading profiles for the 3g FB spectrum are presented in Tables A-V through A-IX. The spectrum is made up of groups of 20 basic flight profiles, each group alternately followed by one of four makeup flight profiles, The total sequence for the 3g FB spectrum is made up as follows:

20 basic flight profiles
Makeup Flight No. 1
20 basic flight profiles
Makeup Flight No. 2
20 basic flight profiles
Makeup Flight No. 3
20 basic flight profiles
Makeup Flight No. 4.

In the evaluation of the fatigue striation patterns, it was noted that the makeup flights exerted negligible influence on the growth rate. Hence, the single basic flight profile was considered to be the reference profile unit for this spectrum.

Special Note. The cyclic frequencies listed in the following tabulations are those characteristic of each flight spectrum. In this experimental program, as discussed in the section entitled "Experimental Details", all tests were conducted under constant frequency conditions. The tests in desiccated or dry air were conducted at 3 Hz, while those in water-saturated JP-4 aircraft fuel were conducted at 2 Hz.

TABLE A-I. 5G SPECTRUM

Layer No.	S_{min}, ksi	S_{max}, ksi	N	Frequency, cpm	Layer No.	S_{min}, ksi	S_{max}, ksi	N	Frequency, cpm
1	27.0	46.1	66	6	30	23.0	75.2	5	6
2	1.5	49.7	34	60	31	23.6	37.3	230	6
3	19.5	24.8	1621	6	32	23.0	31.0	1338	6
4	23.0	33.9	1589	6	33	0.2	57.2	19	60
5	1.3	30.7	1374	60	34	11.1	29.9	1546	60
6	0	25.4	67	60	35	0	18.4	238	60
7	20.4	82.0	1	6	36	1.4	46.4	114	60
8	21.3	65.7	250	6	37	20.4	43.1	370	6
9	0.2	63.8	8	60	38	11.1	59.9	7	60
10	4.7	40.1	2	60	39	5.8	40.0	478	150
11	22.9	100.7	2	6	40	0.2	48.0	63	60
12	10.5	46.3	37	60	41	20.3	77.9	76	6
13	21.8	48.3	367	6	42	1.3	39.5	371	60
14	20.6	73.9	109	6	43	17.0	76.0	37	6
15	22.8	106.6	1	6	44	2.3	50.5	111	60
16	4.7	18.3	265	60	45	30.6	73.2	2	6
17	2.3	59.9	34	60	46	2.2	40.8	363	60
18	22.5	58.1	318	6	47	11.6	82.6	5	6
19	10.6	34.2	6	60	48	10.5	30.7	1280	60
20	0	32.7	21	60	49	19.5	65.9	62	6
21	20.7	51.7	374	6	50	10.5	47.9	1	60
22	5.8	40.0	478	150	51	17.5	50.5	89	6
23	4.6	25.4	46	60	52	24.9	63.0	41	6
24	0.2	34.2	300	60	53	27.9	55.2	57	6
25	4.6	32.6	10	60	54	10.9	40.4	491	60
26	22.8	91.4	4	6	55	0	40.2	6	60
27	0	47.2	4	150	56	11.0	50.4	74	60
28	21.8	41.9	306	6	57	22.7	38.7	682	6
29	23.8	71.8	15	6	58	2.1	29.9	1376	60

TABLE A-II. 7.33G SPECTRUM

Layer No.	S_{min}, ksi	S_{max}, ksi	N	Frequency, cpm	Layer No.	S_{min}, ksi	S_{max}, ksi	N	Frequency, cpm
1	23.3	31.5	1283	6	36	31.5	67.1	2	6
2	10.5	30.9	1280	60	37	30.6	69.4	4	6
3	34.6	49.2	35	6	38	20.2	50.4	84	6
4	10.5	34.3	6	60	39	11.0	60.2	7	60
5	28.5	64.5	1	6	40	20.1	25.3	1529	6
6	23.1	58.5	254	6	41	26.8	64.0	4	6
7	10.5	48.1	1	60	42	20.0	45.6	6	6
8	35.0	49.8	58	6	43	34.6	74.4	1	6
9	5.7	40.1	956	150	44	0	18.4	238	60
10	23.3	32.3	12	6	45	0	57.4	19	60
11	34.7	62.3	7	6	46	11.5	25.7	59	6
12	20.0	31.2	371	6	47	0	40.4	6	60
13	20.2	35.2	150	6	48	23.1	69.5	43	6
14	30.7	41.9	132	6	49	26.8	60.6	6	6
15	11.7	83.1	5	6	50	0.1	34.3	300	60
16	11.1	41.1	301	60	51	16.0	52.6	2	6
17	1.4	30.8	1374	60	52	28.8	39.0	91	6
18	16.1	24.3	43	6	53	15.9	33.1	5	6
19	2.1	50.5	145	60	54	22.9	60.9	30	6
20	26.7	65.9	2	6	55	11.5	33.9	60	6
21	20.3	73.9	98	6	56	23.1	75.5	6	6
22	23.1	45.9	179	6	57	4.7	18.5	265	60
23	23.1	71.3	13	6	58	15.9	53.5	1	6
24	22.9	36.7	84	6	59	23.0	49.2	35	6
25	23.2	80.4	1	6	60	2.2	41.0	363	60
26	20.1	67.5	4	6	61	16.1	31.9	11	6
27	11.5	93.7	2	6	62	16.0	63.4	1	6
28	23.3	50.9	33	6	63	28.8	48.8	21	6
29	11.1	50.5	74	60	64	26.8	46.0	57	6
30	20.4	85.6	2	6	65	20.4	30.8	410	6
31	22.9	91.7	4	6	66	23.3	49.5	160	6
32	23.1	67.1	88	6	67	4.7	32.9	10	60
33	11.5	58.3	18	6	68	23.3	54.9	10	6
34	2.2	30.0	1376	60	69	23.1	34.5	373	6
35	11.5	45.3	31	6	70	10.5	39.7	190	60

TABLE A-II. 7.33G SPECTRUM (Continued)

Layer No.	S_{min}, ksi	S_{max}, ksi	N	Frequency, cpm	Layer No.	S_{min}, ksi	S_{max}, ksi	N	Frequency, cpm
71	22.9	106.7	1	6	93	28.4	68.2	1	6
72	26.7	36.9	212	6	94	26.7	53.7	18	6
73	20.0	36.8	139	6	95	15.9	42.9	3	6
74	11.5	18.5	92	6	96	23.0	101.2	2	6
75	31.4	44.4	52	6	97	0	47.4	4	150
76	1.4	46.6	114	60	98	20.4	52.0	321	6
77	11.1	30.1	1546	60	99	30.7	52.5	36	6
78	20.3	65.1	160	6	100	30.6	73.4	2	6
79	2.2	60.2	34	60	101	30.5	75.7	1	6
80	10.5	46.5	37	60	102	20.4	82.2	9	6
81	20.2	43.0	121	6	103	20.1	56.7	44	6
82	28.7	57.9	6	6	104	20.4	78.2	62	6
83	30.6	62.0	11	6	105	11.5	70.7	12	6
84	22.9	77.9	11	6	106	35.2	74.4	2	6
85	0.2	48.2	63	60	107	20.2	61.6	7	6
86	4.7	40.3	1	60	108	35.1	83.7	1	6
87	1.4	39.6	371	60	109	20.4	40.4	238	6
88	20.0	40.0	20	6	110	0	25.6	67	60
89	4.7	25.5	46	60	111	0.1	64.1	8	60
90	16.1	41.9	7	6	112	35.1	63.1	11	6
91	20.4	79.6	26	6	113	23.3	49.7	319	6
92	31.5	55.9	10	6	114	0	32.8	21	60
					115	20.2	47.2	138	6

TABLE A-III. 5G SPECTRUM WITH COMPRESSION

Layer No.	S_{min}, ksi	S_{max}, ksi	N	Frequency, cpm	Layer No.	S_{min}, ksi	S_{max}, ksi	N	Frequency, cpm
1	27.0	46.1	66	6	36	23.0	75.2	5	6
2	1.5	49.7	34	60	37	23.6	37.3	230	6
3	19.5	24.8	1621	6	38	23.0	31.0	1338	6
4	20.4	82.2	5		39	0.2	57.2	19	60
5	23.0	33.9	1589	6	40	11.1	29.9	1546	60
6	20.4	85.6	2		41	0	18.4	238	60
7	1.3	30.7	1374	60	42	1.4	46.4	114	60
8	22.9	108.3	1		43	20.4	43.1	370	6
9	0	25.4	67	60	44	11.1	59.9	7	60
10	20.4	82.0	1	6	45	5.8	40.0	478	150
11	21.3	65.7	250	6	46	0.2	48.0	63	60
12	-20.0	93.7	1		47	20.3	77.9	76	6
13	0.2	63.8	8	60	48	1.3	39.5	371	60
14	11.5	93.7	1		49	17.0	76.0	37	6
15	4.7	40.1	2	60	50	2.3	50.5	111	60
16	22.9	100.7	2	6	51	30.6	73.2	2	6
17	10.5	46.3	37	60	52	2.2	40.8	363	60
18	21.8	48.3	367	6	53	11.6	82.6	5	6
19	28.0	102.3	1		54	10.5	30.7	1280	60
20	20.6	73.9	109	6	55	23.2	80.4	1	
21	22.8	106.6	1	6	56	19.5	65.9	62	6
22	4.7	18.3	265	60	57	10.5	47.9	1	60
23	2.3	59.9	34	60	58	17.5	50.5	89	6
24	22.5	58.1	318	6	59	20.4	90.2	1	
25	10.6	34.2	6	60	60	24.9	63.0	41	6
26	-4.0	32.7	21	60	61	27.9	55.2	57	6
27	20.7	51.7	374	6	62	10.9	40.4	491	60
28	5.8	40.0	478	150	63	10.2	51.6	7	
29	4.6	25.4	46	60	64	0	40.2	6	60
30	0.2	34.2	300	60	65	11.0	50.4	74	60
31	4.6	32.6	10	60	66	22.7	38.7	682	6
32	22.8	91.4	4	6	67	-12.0	67.5	4	
33	0	47.2	4	150	68	2.1	29.9	1376	60
34	21.8	41.9	306	6	69	20.4	82.2	5	
35	23.8	71.8	15	6					

TABLE A-IV. 5g CTB SPECTRUM

Layer No.	S_{min}, ksi	S_{max}, ksi	N	Frequency, cpm	Layer No.	S_{min}, ksi	S_{max}, ksi	N	Frequency, cpm
1	18.6	45.4	144	120	35	8.8	38.5	497	120
2	27.3	38.5	212	120	36	33.4	49.8	35	60
3	18.7	27.7	1960	150	37	18.1	75.4	99	120
4	29.0	51.9	21	60	38	29.3	40.6	91	120
5	26.0	76.3	145	120	39	25.7	37.3	1367	150
6	7.6	27.3	33	60	40	9.3	15.0	66	60
7	18.5	35.0	518	120	41	33.2	72.1	7	60
8	0	58.5	34	60	42	17.9	64.0	160	120
9	7.6	40.0	14	60	43	0.3	28.5	2777	150
10	40.2	57.5	58	60	44	25.9	103.5	4	60
11	7.8	34.0	18	60	45	26.2	113.8	2	60
12	31.3	66.5	11	60	46	7.6	21.2	70	60
13	31.8	44.8	184	120	47	17.7	76.9	1	60
14	25.8	66.2	294	120	48	18.5	71.0	98	120
15	8.9	29.6	1291	150	49	25.8	45.2	692	120
16	33.4	85.6	1	60	50	7.7	45.2	5	60
17	27.4	59.8	24	60	51	31.7	73.7	6	60
18	26.2	55.6	407	120	52	7.5	16.3	105	120
19	27.4	49.0	57	60	53	28.7	71.7	2	60
20	0	38.5	1034	150	54	40.1	72.9	11	60
21	31.3	56.9	46	60	55	18.5	50.4	459	120
22	9.0	47.1	111	120	56	29.3	62.3	6	60
23	0	64.8	19	60	57	8.8	58.5	6	60
24	33.2	97.7	1	60	58	40.3	85.6	2	60
25	26.2	87.3	16	60					
26	27.6	70.6	6	60					
27	6.0	35.7	966	150					
28	31.6	81.2	4	60					
29	0.3	12.5	305	120					
30	11.6	21.3	15	60					
31	9.1	27.5	1549	150					
32	7.5	11.7	357	120					
33	0	48.3	375	120					
34	0	71.9	8	60					

TABLE A-V. 3.0G FB FLIGHT BY FLIGHT SPECTRUM (BASIC MISSION)

Layer No.	σ_{min}, ksi	σ_{max}, ksi	N	Frequency, cpm	Layer No.	σ_{min}, ksi	σ_{max}, ksi	N	Frequency, cpm
1	0	0			30	9.6	25.5	9	150
2	14.0	29.8	1	150	31	5.6	29.4	8	150
3	12.5	31.3	1	150	32	12.0	40.6	1	6
4	14.0	32.8	1	150	33	2.3	32.7	10	150
5	23.0	39.1	3	6	34	11.2	29.7	2	6
6	12.5	31.3	1	150	35	6.7	28.4	9	150
7	20.4	35.0	1	6	36	9.6	25.5	9	150
8	21.6	39.7	1	6	37	8.1	26.9	9	150
9	3.7	25.5	2	6	38	9.6	25.5	9	150
10	9.6	25.5	9	150	39	-3.4	38.5	1	150
11	6.7	28.4	9	150	40	8.1	26.9	26	150
12	5.6	29.4	8	150	41	0	28.9	5	6
13	3.8	31.3	9	150	42	8.1	26.9	8	150
14	9.6	25.5	9	150	43	9.6	25.5	9	150
15	8.1	26.9	9	150	44	5.6	29.4	7	150
16	6.7	28.4	9	150	45	-.5	18.0	4	6
17	9.6	25.5	18	150	46	9.6	25.5	9	150
18	8.1	26.9	9	150	47	8.1	26.9	8	150
19	-2.0	37.0	1	150	48	6.7	28.4	9	150
20	9.6	25.5	9	150	49	9.6	25.5	8	150
21	5.6	29.4	8	150	50	17.0	35.5	2	6
22	9.6	25.5	18	150	51	9.6	25.5	8	150
23	5.4	23.8	3	6	52	6.7	28.4	8	150
24	-5.5	23.0	2	6	53	9.6	25.5	8	150
25	9.6	25.5	9	150	54	6.2	34.7	3	6
26	7.8	33.0	1	6	55	9.6	25.5	8	150
27	6.7	28.4	9	150	56	8.1	26.9	8	150
28	2.0	27.2	1	6	57	-4.9	39.9	1	150
29	8.1	26.9	9	150	58	.9	34.1	5	150

TABLE A-V. 3.0G FB FLIGHT BY FLIGHT SPECTRUM (BASIC MISSION) (Continued)

Layer No.	σ_{min}, ksi	σ_{max}, ksi	N=	Frequency, cpm	Layer No.	σ_{min}, ksi	σ_{max}, ksi	N	Frequency, cpm
59	9.6	25.5	16	150	86	35.9	57.6	55	150
60	3.8	31.3	8	150	87	38.8	54.7	16	150
61	-.5	35.6	4	150	88	37.3	56.1	35	150
62	-2.2	19.7	2	6	89	33.0	60.5	62	150
63	8.1	26.9	8	150	90	37.3	56.1	44	150
64	-.3	15.6	2	150	91	34.8	58.6	58	150
65	1.7	17.1	1	150	92	38.8	54.7	45	150
66	8.8	8.8			93	34.8	58.6	59	150
67	8.4	27.4	1	6	94	37.3	56.1	50	150
68	12.5	28.4	2	150	95	38.8	54.7	98	150
69	11.0	29.8	1	150	96	37.3	56.1	39	150
70	9.6	31.3	1	150	97	34.8	58.6	60	150
71	37.3	56.1	40	150	98	37.3	56.1	166	150
72	38.8	54.7	2	150	99	36.6	52.5	27	150
73	31.5	61.9	63	150	100	35.1	53.9	46	150
74	38.8	54.7	20	150	101	36.6	52.5	62	150
75	47.5	66.4	64	6	102	33.7	55.4	51	150
76	35.9	57.6	56	150	103	35.1	53.9	48	150
77	38.8	54.7	22	150	104	33.7	55.4	54	150
78	37.3	56.1	49	150	105	36.6	52.5	48	150
79	38.8	54.7	29	150	106	33.7	55.4	57	150
80	37.3	56.1	42	150	107	36.6	52.5	103	150
81	38.8	54.7	34	150	108	35.1	53.9	41	150
82	35.9	57.6	52	150	109	36.6	52.5	30	150
83	38.8	54.7	32	150	110	32.6	56.5	61	150
84	37.3	56.1	37	150	111	35.1	53.9	43	150
85	38.8	54.1	27	150	112	33.7	55.4	53	150
					113	0	0		

TABLE A-VI. 3.0G FB FLIGHT-BY-FLIGHT SPECTRUM (MAKEUP FLIGHT NO. 1)

Layer No.	σ_{min}, ksi	σ_{max}, ksi	N	Frequency, cpm	Layer No.	σ_{min}, ksi	σ_{max}, ksi	N	Frequency, cpm
1	51.1	80.3	2	6	32	.3	28.9	5	6
2	56.2	75.2	2	6	33	22.6	48.9	2	6
3	52.9	78.5	1	6	34	12.4	38.7	5	6
4	55.5	75.9	6	6	35	6.3	22.9	3	6
5[a]	.9	42.9	1	150	36	16.9	59.8	2	6
6	3.8	40.0	1	150	37	13.8	32.2	3	6
7	5.3	38.5	1	150	38	-2.2	22.6	5	6
8	11.1	32.7	1	150	39	10.1	46.1	2	6
9	6.7	37.1	1	150	40	-12.4	12.4	5	6
10[b]	9.6	34.2	4	150	41	6.1	29.7	4	6
11	8.2	35.6	2	150	42	23.1	43.3	2	6
12	21.9	47.5	1	6	43	-6.8	22.1	2	6
13[a]	6.7	37.1	1	150	44	-.6	18.2	1	150
14	12.5	34.2	2	150	45	8.8	36.5	4	6
15[a]	24.4	59.5	1	6	46[a]	19.3	57.3	1	6
16	24.6	52.1	2	6	47	-2.1	23.5	2	150
17	11.1	35.6	2	150	48[a]	8.8	56.9	1	6
18	23.8	45.6	8	6	49	10.6	45.6	1	6
19	9.6	37.1	1	150	50	12.4	35.8	9	6
20	9.6	34.2	2	150	51	19.4	47.0	1	6
21[b]	11.1	32.7	2	150	52	7.4	34.9	4	150
22	6.7	37.1	1	150	53	3.1	39.2	1	150
23	8.2	35.6	1	150	54	6.0	36.3	3	150
24[a]	3.8	40.0	1	150	55[a]	-2.7	45.0	1	150
25	-5.5	23.0	11	6	56	4.5	37.8	2	150
26	15.4	37.2	10	6	57	1.7	40.7	1	150
27[a]	14.5	49.7	1	6	58	8.9	33.5	6	150
28	13.7	38.9	1	6	59	30.1	63.3	5	150
29	23.7	52.2	1	6	60	28.7	64.8	3	150
30[a]	13.7	38.9	1	6	61[a]	30.1	63.3	2	150
31	2.0	27.2	3	6	62	27.2	66.2	1	150
					63	25.8	67.7	1	150

(a) Layers unique to that particular makeup flight. All other layers are common to each makeup flight.

(b) Layers which are common to all makeup flights, but include an additional single cycle which is unique to that particular makeup flight.

TABLE A-VII. 3.0G FB FLIGHT-BY-FLIGHT SPECTRUM
(MAKEUP FLIGHT NO. 2)

Layer No.	σ_{min}, ksi	σ_{max}, ksi	N	Frequency, cpm	Layer No.	σ_{min}, ksi	σ_{max}, ksi	N	Frequency, cpm
1	51.1	80.3	2	6	33	2.0	27.2	3	6
2	56.2	75.2	2	6	34	.3	28.9	5	6
3	52.9	78.5	1	6	35	22.6	48.9	2	6
4	55.5	75.9	6	6	36	12.4	38.7	5	6
5	3.8	40.0	1	150	37	6.3	22.9	3	6
6	5.3	38.5	1	150	38	16.9	59.8	2	6
7[a]	2.4	41.4	1	150	39	13.8	32.2	3	6
8	11.1	32.7	1	150	40	-2.2	22.6	5	6
9	6.7	37.1	1	150	41	10.1	46.1	2	6
10	9.6	34.2	3	150	42	-12.4	12.4	5	6
11	8.2	35.6	2	150	43	6.1	29.7	4	6
12[a]	2.4	41.4	1	150	44	23.1	43.3	2	6
13	21.9	47.5	1	6	45	-6.8	22.1	2	6
14[a]	5.3	41.4	1	150	46	-.6	18.2	1	150
15	12.5	34.2	2	150	47[a]	-5.0	22.5	1	150
16[a]	21.7	54.9	1	6	48	8.8	36.5	4	6
17	24.6	52.1	2	6	49[a]	-3.5	21.0	1	150
18	11.1	35.6	2	150	50	-2.1	23.5	2	150
19	23.8	45.6	8	6	51	10.6	45.6	1	6
20	9.6	37.1	1	150	52	12.4	35.8	9	6
21[a]	11.1	32.7	1	150	53	19.4	47.0	1	6
22	9.6	34.2	2	150	54	7.4	34.9	4	150
23	11.1	32.7	1	150	55	3.1	39.2	1	150
24	6.7	37.1	1	150	56	6.0	36.3	3	150
25[a]	2.4	41.4	1	150	57	4.5	37.8	2	150
26	8.2	35.6	1	150	58[a]	.2	42.1	1	150
27[a]	23.7	52.2	1	6	59	1.7	40.7	1	150
28	-5.5	23.0	11	6	60	8.9	33.5	6	150
29	15.4	37.2	10	6	61[a]	1.7	40.7	1	150
30	13.7	38.9	1	6	62	30.1	63.3	5	150
31	23.7	52.2	1	6	63	28.7	64.8	3	150
32	17.0	58.9	1	6	64	27.2	66.2	1	150
					65	25.8	67.7	1	150

(a) Layers unique to that particular makeup flight. All other layers are common to each makeup flight.

TABLE A-VIII. 3.0G FB FLIGHT-BY-FLIGHT SPECTRUM (MAKEUP FLIGHT NO. 3)

Layer No.	σ_{min}, ksi	σ_{max}, ksi	N	Frequency, cpm	Layer No.	σ_{min}, ksi	σ_{max}, ksi	N	Frequency, cpm
1	51.1	80.3	2	6	33[a]	14.5	49.7	1	6
2	56.2	75.2	2	6	34	22.6	48.9	2	6
3	52.9	78.5	1	6	35	12.4	38.7	5	6
4	55.5	75.9	6	6	36	6.3	22.9	3	6
5	3.8	40.0	1	150	37	16.9	59.8	2	6
6	5.3	38.5	1	150	38	13.8	32.2	3	6
7	11.1	32.7	1	150	39	-2.2	22.6	5	6
8[b]	6.7	37.1	2	150	40	10.1	46.1	2	6
9[a]	.5	44.3	1	150	41	-12.4	12.4	5	6
10	9.6	34.2	3	150	42	6.1	29.7	4	6
11	8.2	35.6	2	150	43	23.1	43.3	2	6
12[a]	8.2	38.5	1	150	44	-6.8	22.1	2	6
13	21.9	47.5	1	6	45[a]	-2.1	23.5	1	150
14[a]	21.7	54.9	1	6	46	-.6	18.2	1	150
15	12.5	34.2	2	150	47[a]	-2.1	23.5	1	150
16	24.6	52.1	2	6	48	8.8	36.5	4	6
17	11.1	35.6	2	150	49	-2.1	23.5	2	150
18	23.8	45.6	8	6	50	10.6	45.6	1	6
19	9.6	37.1	1	150	51	12.4	35.8	9	6
20	9.6	34.2	2	150	52	19.4	47.0	1	6
21[a]	5.3	38.5	1	150	53	7.4	34.9	4	150
22	11.1	32.7	1	150	54	3.1	39.2	1	150
23	6.7	37.1	1	150	55[a]	-4.1	46.5	1	150
24[a]	5.3	38.5	1	150	56	6.0	36.3	3	150
25	8.2	35.6	1	150	57	4.5	37.8	2	150
26	-5.5	23.0	11	6	58	1.7	40.7	1	150
27	15.4	37.2	10	6	59	8.9	33.5	6	150
28	13.7	38.9	1	6	60	30.1	63.3	5	150
29	23.7	52.2	1	6	61[a]	24.3	69.1	1	150
30	2.0	27.2	3	6	62	28.7	64.8	3	150
31[a]	13.7	38.9	1	6	63	27.2	66.2	1	150
32	.3	28.9	5	6	64	25.8	67.7	1	150

(a) Layers unique to that particular makeup flight. All other layers are common to each make-up flight.

(b) Layers which are common to all makeup flights but include an additional single cycle which is unique to that particular makeup flight.

TABLE A-IX. 3.0G FB FLIGHT-BY-FLIGHT SPECTRUM
(MAKEUP FLIGHT NO. 4)

Layer No.	σ_{min}, ksi	σ_{max}, ksi	N	Frequency, cpm	Layer No.	σ_{min}, ksi	σ_{max}, ksi	N	Frequency, cpm
1	51.1	80.3	2	6	33	12.4	38.7	5	6
2	56.2	75.2	2	6	34	6.3	22.9	3	6
3	52.9	78.5	1	6	35	16.9	59.8	2	6
4	55.5	75.9	6	6	36	13.8	32.2	3	6
5[a]	9.6	34.2	1	150	37	-2.2	22.6	5	6
6	3.8	40.0	1	150	38	10.1	46.1	2	6
7	5.3	38.5	1	150	39	-12.4	12.4	5	6
8	11.1	32.7	1	150	40	6.1	29.7	4	6
9[b]	6.7	37.1	2	150	41	23.1	43.3	2	6
10	9.6	34.2	3	150	42	-6.8	22.1	2	6
11	8.2	35.6	2	150	43	-.6	18.2	1	150
12	21.9	47.5	1	6	44[a]	16.2	48.1	1	6
13	12.5	34.2	2	150	45	8.8	36.5	4	6
14	24.6	52.1	2	6	46[a]	23.7	52.2	1	6
15	11.1	35.6	2	150	47	-2.1	23.5	2	150
16[a]	5.3	38.5	1	150	48	10.6	45.6	1	6
17	23.8	45.6	8	6	49	12.4	35.8	9	6
18	9.6	37.1	1	150	50[a]	27.0	48.9	1	6
19[a]	3.8	37.1	1	150	51	19.4	47.0	1	6
20	9.6	34.2	2	150	52	7.4	34.9	4	150
21[a]	.9	42.9	1	150	53[a]	.2	42.1	1	150
22	11.1	32.7	1	150	54	3.1	39.2	1	150
23	6.7	37.1	1	150	55	6.0	36.3	3	150
24	8.2	35.6	1	150	56	4.5	37.8	2	150
25	-5.5	23.0	11	6	57[a]	-1.2	43.6	1	150
26[a]	16.2	48.1	1	6	58	1.7	40.7	1	150
27	15.4	37.2	10	6	59	8.9	33.5	6	150
28	13.7	38.9	1	6	60	30.1	63.3	5	150
29	23.7	52.2	1	6	61[a]	27.2	66.2	1	150
30	2.0	27.2	3	6	62	28.7	64.8	3	150
31	.3	28.9	5	6	63	27.2	66.2	1	150
32	22.6	48.9	2	6	64	25.8	67.7	1	150

(a) Layers unique to that particular makeup flight. All other layers are common to each makeup flight.

(b) Layers which are common to all makeup flights but includes an additional single cycle which is unique to that particular makeup flight.

APPENDIX B

STRIATION MEASUREMENTS FROM FLIGHT LOAD SPECTRUM TESTS

APPENDIX B

STRIATION MEASUREMENTS FROM FLIGHT LOAD SPECTRUM TESTS

The striation measurements obtained from the photomacrographs of Figures 5 through 12 are tabulated in this appendix. Because the crack growth at the specimen surface is somewhat less than that slightly below the surface, the measurement scheme illustrated below has been adopted to characterize the flaw shape.

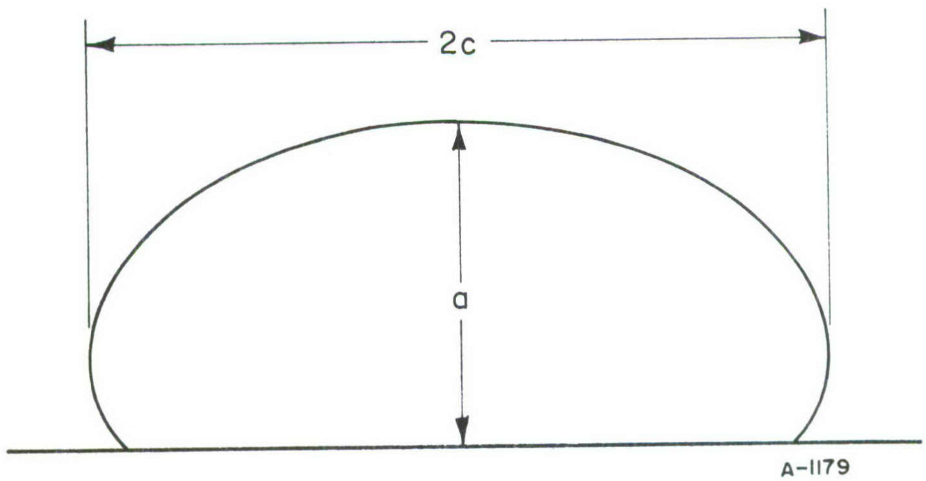

SURFACE CRACK DIMENSIONS

Following each tabulation, a crack growth curve for that tabulation is presented. The crack growth curves for the two final tabulations are combined on one figure since surface flaw detail was distinguishable only on one specimen.

These tabulations represent the total number of profiles applied to the specimen. The early profile markings were generally unclear, and, hence, are not reported. On the figures, the dashed lines indicate the probable early growth trend. It should be noted that when fracture occurred in one profile, the number of "completed" profiles, as reported in Table 5 of the main report, is one profile less.

TABLE B-I. STRIATION MEASUREMENTS FOR SPECIMEN 3

Load Profiles No.	Crack Depth a inch	Maximum Crack Length 2c inch	Remarks
0	0.090	0.126	Estimated
21	0.129	0.184	
26	0.140	0.220	
31	0.155	0.221	
36	0.172	0.245	
37	0.177	0.253	
38	0.181	0.260	
39	0.186	0.286	
40	0.191	0.294	
41	0.196	0.304	
42	0.201	0.316	
43	0.206	0.324	
44	0.212	0.334	
45	0.218	0.343	
46	0.225	0.359	
47	0.232	0.375	
48	0.240	0.388	
49	0.247	0.400	
50	0.255	0.412	
51	0.263	0.432	
52	0.273	0.450	
53	0.283	0.465	
54	0.294	0.484	
55	0.305	0.501	
56	0.317	0.525	
57	0.331	0.552	
58	0.347	0.596	
59	0.365	0.635	
60	0.384	0.682	
61	0.405	0.738	Fracture

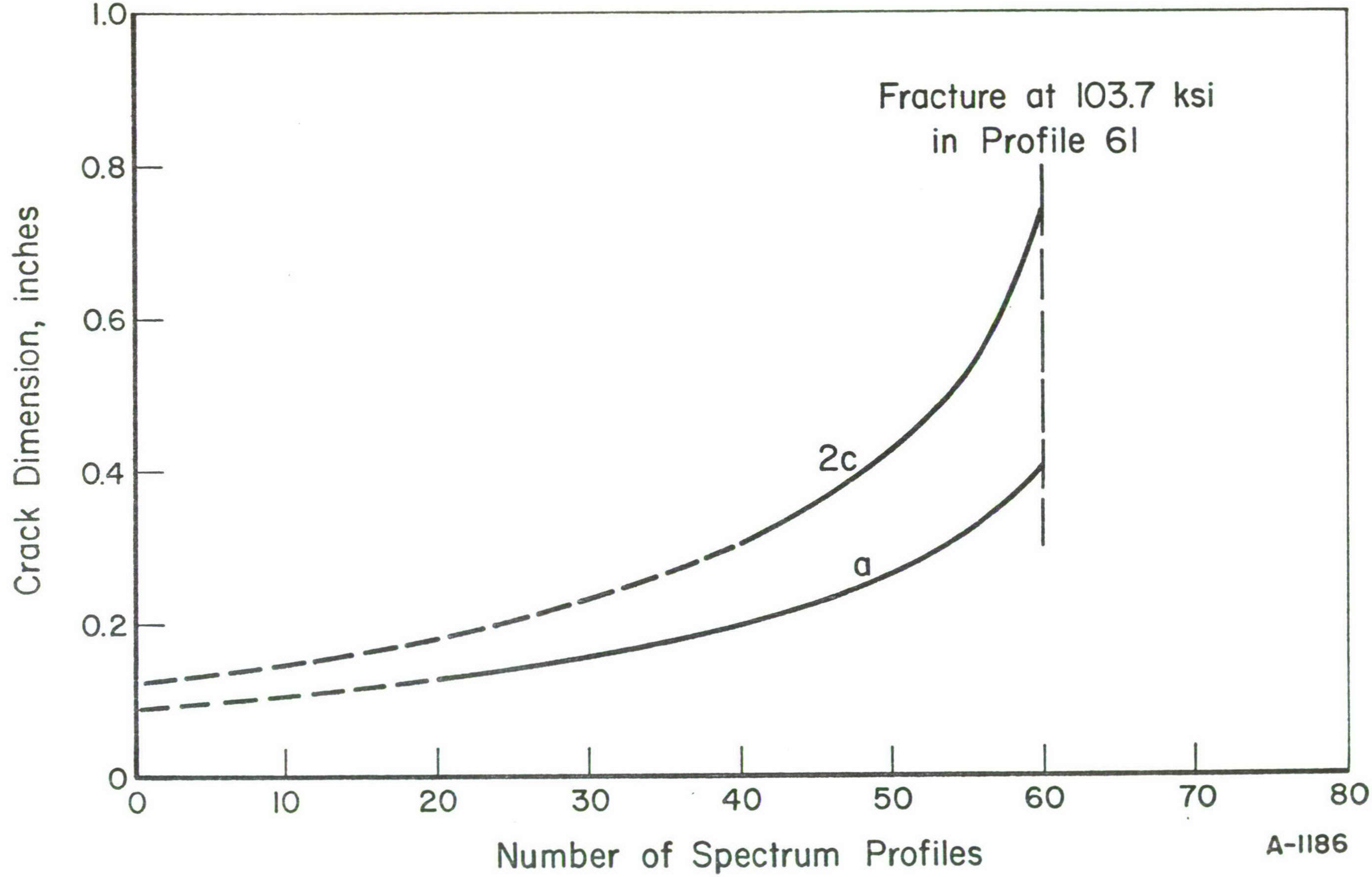

FIGURE B-1. CRACK GROWTH IN 5g MAC SPECTRUM IN DRY AIR

TABLE B-II. STRIATION MEASUREMENTS FOR SPECIMEN 6

Load Profiles No.	Crack Depth a inch	Maximum Crack Length 2c inch	Remarks
0	.089	.150	
76	.175	.271	
77	.183	.284	
78	.189	.293	
79	.197	.305	
80	.204	.316	
81	.213	.330	
82	.220	.343	
83	.230	.357	
84	.239	.376	
85	.248	.392	
86	.259	.410	
87	.268	.427	
88	.279	.448	
89	.291	.469	
90	.303	.491	
91	.316	.517	
92	.329	.542	
93	.345	.570	
94	.360	.615	
95	.377	.637	
96	.396	.678	
97	.415	.725	
98	.436	.779	
99	.461	.844	
100	.490	.922	Fracture

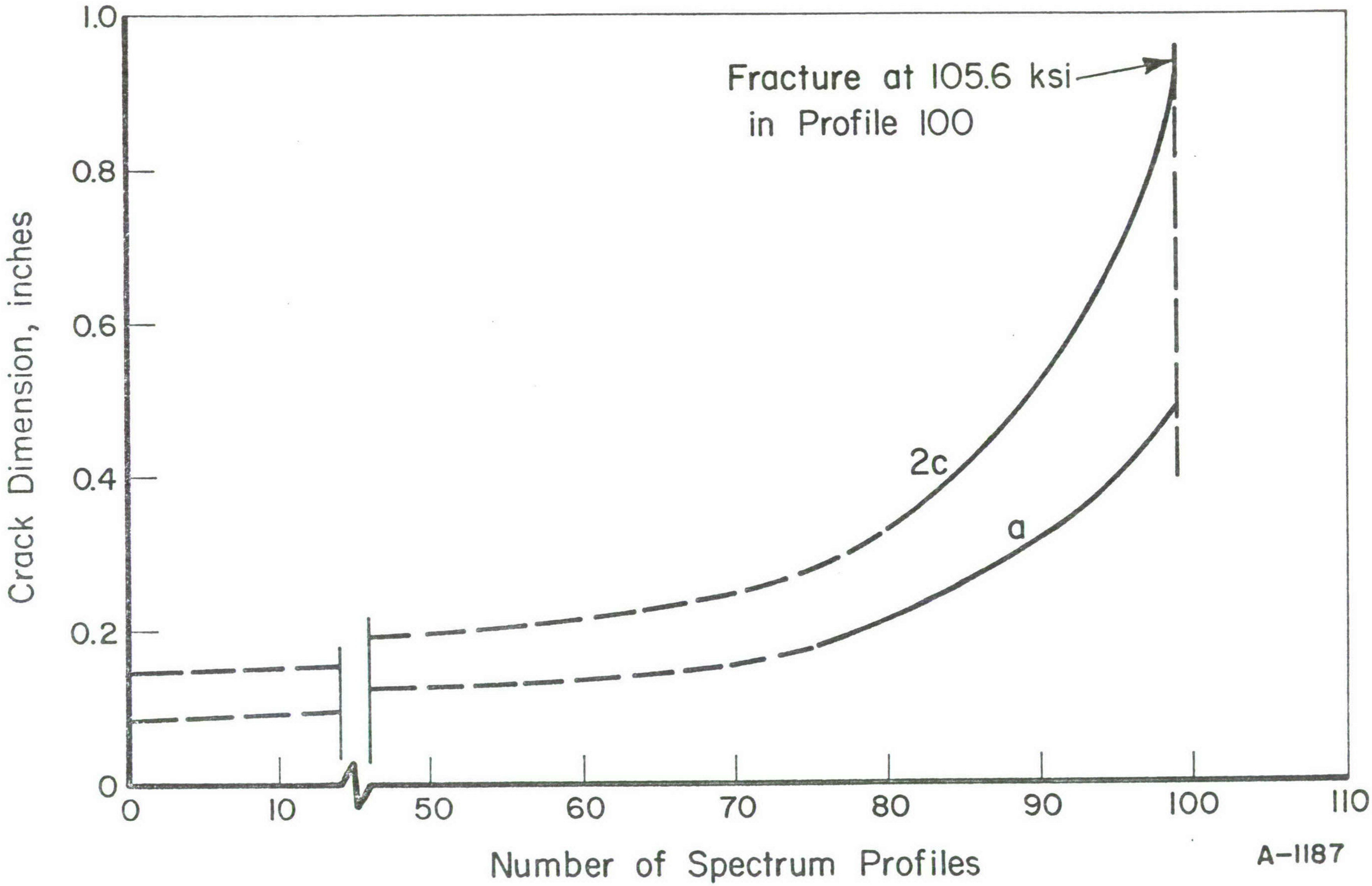

FIGURE B-2. CRACK GROWTH IN 5g MAC SPECTRUM IN JP-4

TABLE B-III. STRIATION MEASUREMENTS FOR SPECIMEN 9

Applied Load Profile No.	Crack Depth a inch	Maximum Crack Length 2c inch	Remarks
0	.088	.167	
18	.147	.262	
19	.152	.271	
20	.158	.282	
21	.164	.293	
22	.170	.304	
23	.174	.311	
24	.180	.322	
25	.189	.338	
26	.197	.352	
27	.204	.364	
28	.211	.383	
29	.220	.396	
30	.228	.413	
31	.237	.430	
32	.244	.449	
33	.256	.469	
34	.264	.485	
35	.278	.504	
36	.290	.526	
37	.304	.551	
38	.318	.581	
39	.334	.611	
40	.352	.648	
41	.370	.686	Fracture

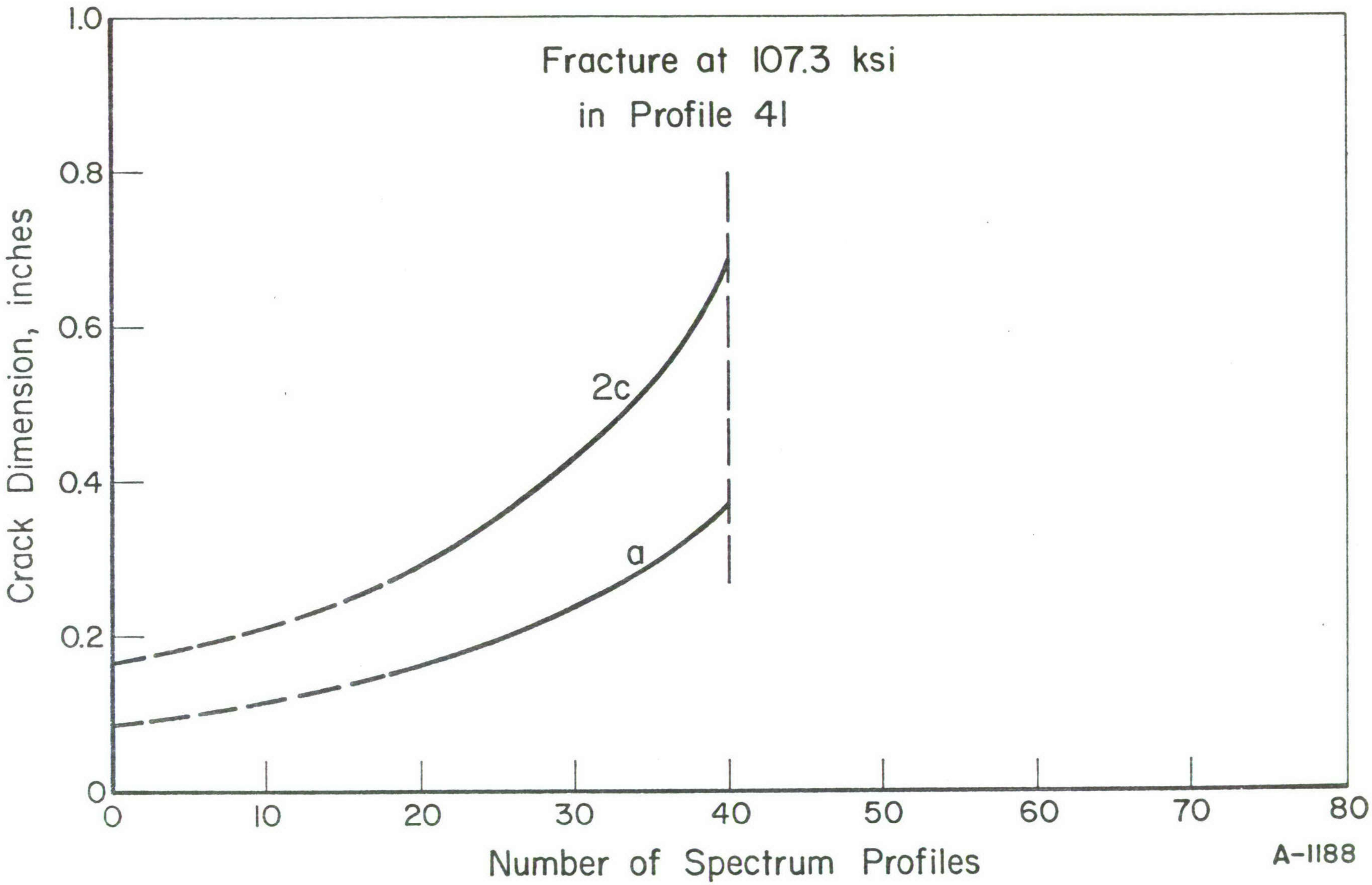

FIGURE B-3. CRACK GROWTH IN 5g MAC SPECTRUM WITH COMPRESSION IN JP-4

TABLE B-IV. STRIATION MEASUREMENTS FOR SPECIMEN 4

Applied Load Profile No.	Flaw Depth a inch	Maximum Flaw Length 2c inch	Remarks
0	.110	.194	Estimated
30	.231	.394	
31	.234	.400	
32	.246	.425	
33	.255	.441	
34	.265	.459	
35	.272	.470	
36	.281	.486	
37	.289	.500	
38	.298	.518	
39	.308	.540	
40	.322	.565	
41	.335	.585	
42	.350	.614	
43	.364	.639	
44	.381	.667	
45	.401	.703	
46	.425	.745	
47	.432	.812	Fracture

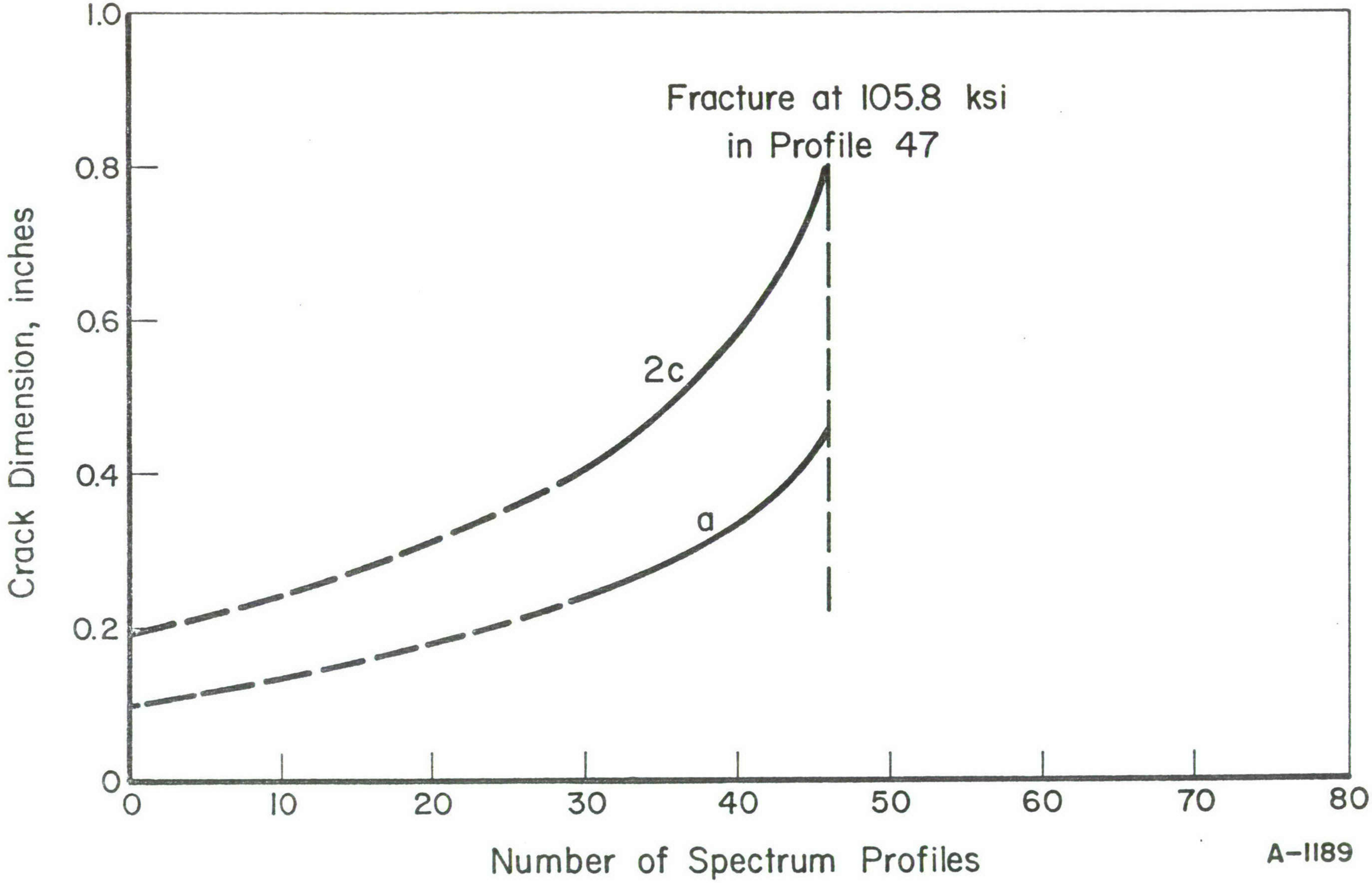

FIGURE B-4. CRACK GROWTH IN 7.33g MAC SPECTRUM IN DRY AIR

TABLE B-V. STRIATION MEASUREMENTS FOR SPECIMEN 8

Applied Load Profile No.	Flaw Depth a inch	Maximum Flaw Length 2c inch	Remarks
0	.078	.140	
35	.173	.304	
36	.179	.314	
37	.189	.332	
38	.196	.344	
39	.202	.355	
40	.208	.366	
41	.215	.377	
42	.221	.389	
43	.229	.403	
44	.237	.417	
45	.245	.433	
46	.254	.449	
47	.262	.465	
48	.273	.483	
49	.284	.502	
50	.294	.525	
51	.306	.548	
52	.319	.573	
53	.333	.601	
54	.348	.630	
55	.366	.666	
56	.384	.704	
57	.406	.747	
58	.431	.804	Fracture

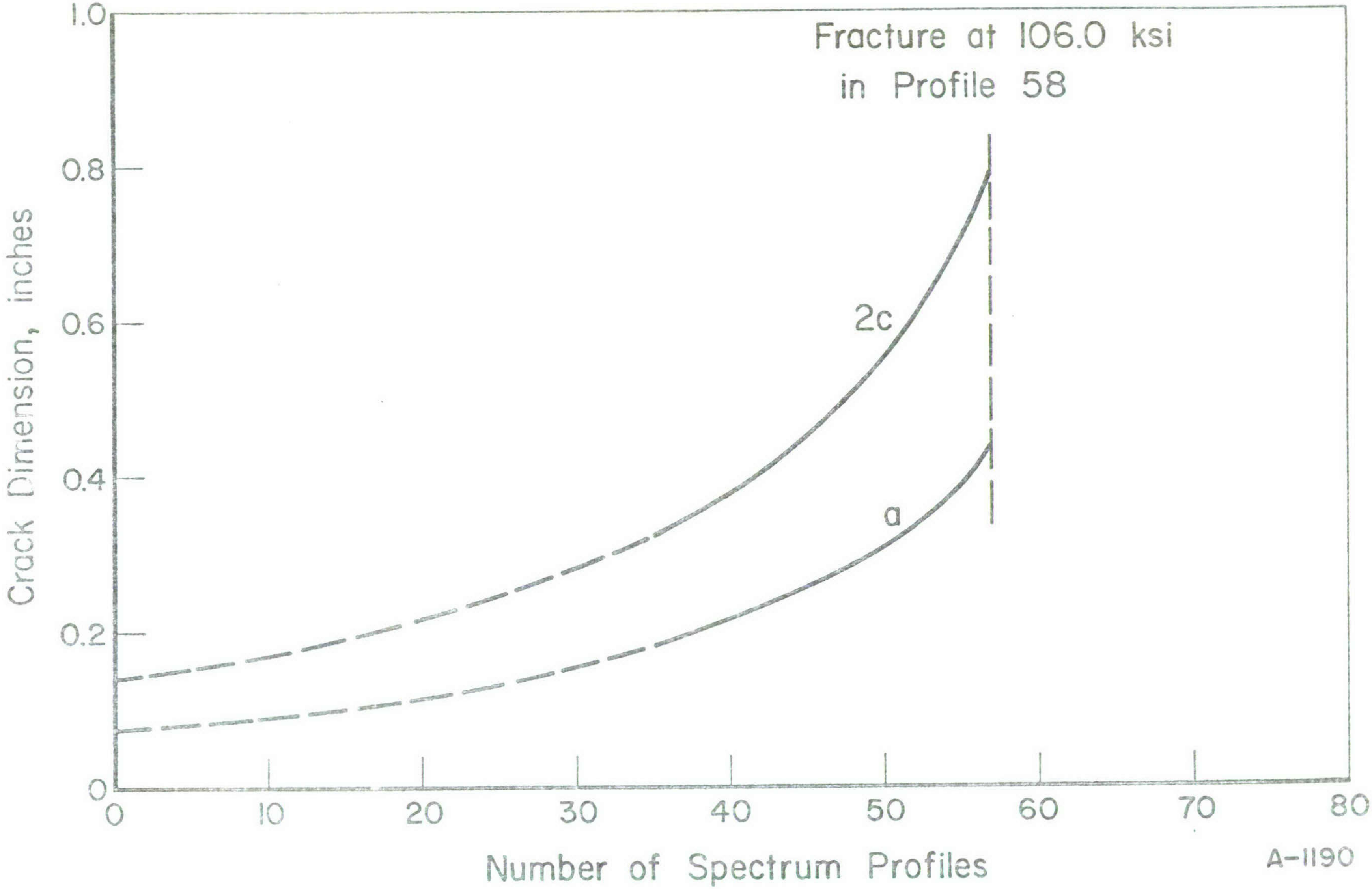

FIGURE B-5. CRACK GROWTH IN 7.33g MAC SPECTRUM IN JP-4

TABLE B-VI. STRIATION MEASUREMENTS FOR SPECIMEN 10

Applied Load Profile No.	Flaw Depth a inch	Maximum Flaw Length 2c inch	Remarks
0	.082	.146	
21	.132	.222	
22	.135	.228	
23	.139	.233	
24	.143	.241	
25	.147	.248	
26	.151	.255	
27	.155	.262	
28	.160	.270	
29	.163	.275	
30	.169	.285	
31	.173	.292	
32	.179	.302	
33	.184	.310	
34	.190	.320	
35	.195	.329	
36	.201	.339	
37	.208	.351	
38	.214	.361	
39	.221	.372	
40	.228	.385	
41	.235	.396	
42	.245	.419	
43	.253	.433	
44	.261	.446	
45	.272	.465	
46	.282	.482	
47	.292	.499	
48	.304	.520	
49	.314	.537	
50	.328	.560	
51	.341	.584	
52	.356	.615	
53	.372	.642	
54	.391	.675	
55	.411	.724	
56	.436	.780	
57	.461	.852	
58	.494	.972	
59	.528	1.064	Fracture

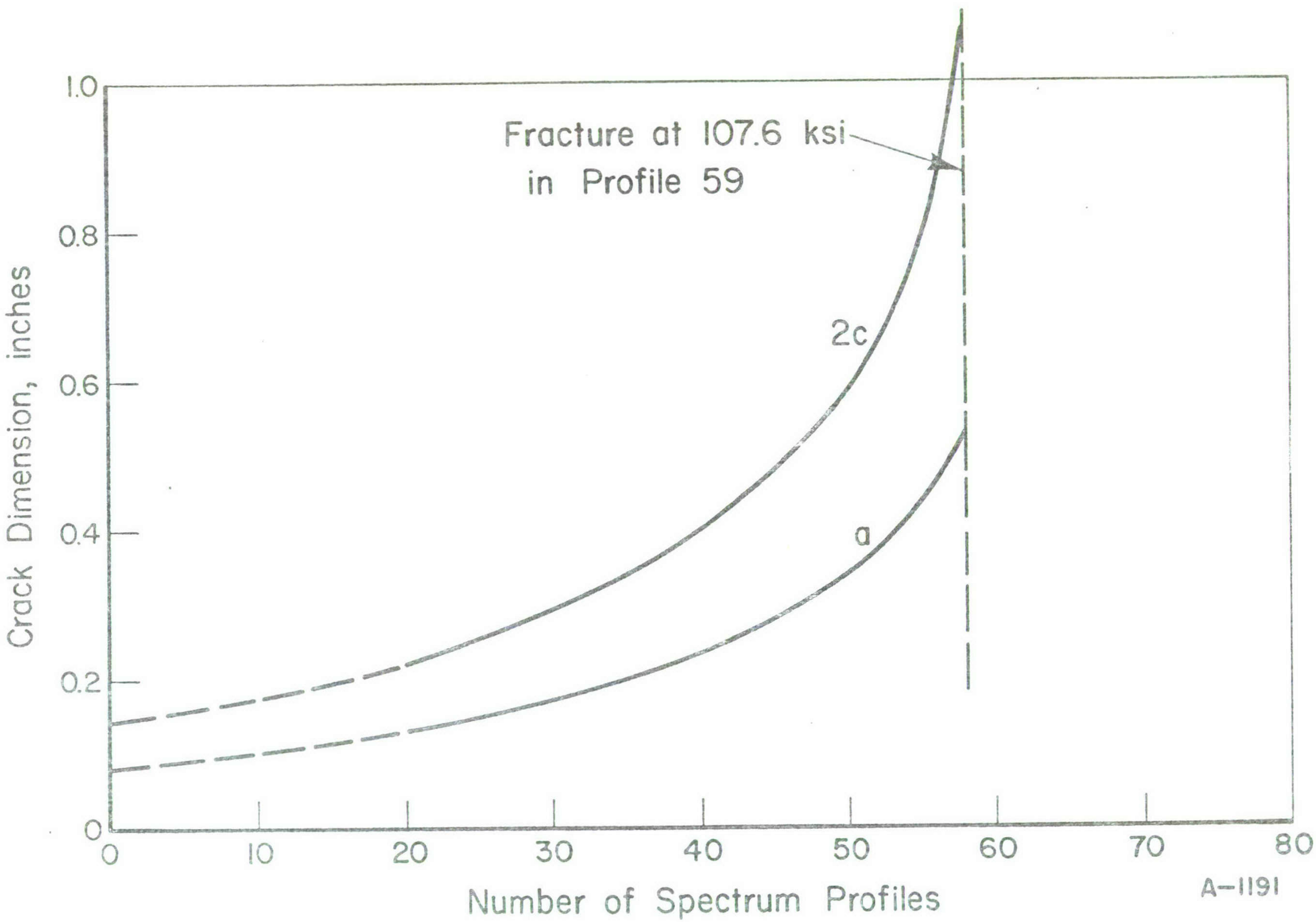

FIGURE B-6. CRACK GROWTH IN 5g CTB SPECTRUM IN JP-4

TABLE B-VII. STRIATION MEASUREMENTS FOR SPECIMEN 11

No. of Load Profiles Applied	Crack Depth a inch	Maximum Crack Length 2c inch	Remarks
0	.080	.160	
80	.177	.399	
85	.190	.429	
90	.202	.455	
91	.205	.461	
92	.207	.466	
93	.211	.475	
94	.214	.482	
95	.217	.489	
96	.220	.495	
97	.223	.502	
98	.227	.511	
99	.230	.518	
100	.233	.525	
101	.239	.535	
102	.243	.547	
103	.247	.556	
104	.251	.565	
105	.256	.576	
106	.261	.588	
107	.267	.601	
108	.273	.615	
109	.279	.629	
Surface Crack Broke Through Back Surface			
112	---	.66	
113	---	.70	
114	---	.73	
115	---	.76	
116	---	.80	
117	---	.87	
118	---	.94	
119	---	.00	
120	---	1.06	
121	---	1.15	
122	---	1.26	
123	---	1.40	
124	---	1.60	
125	---	1.76	
126	---	1.92	
127	---	2.16	
128	---	2.40	
129	---	2.74	
130	---	2.80	Fracture

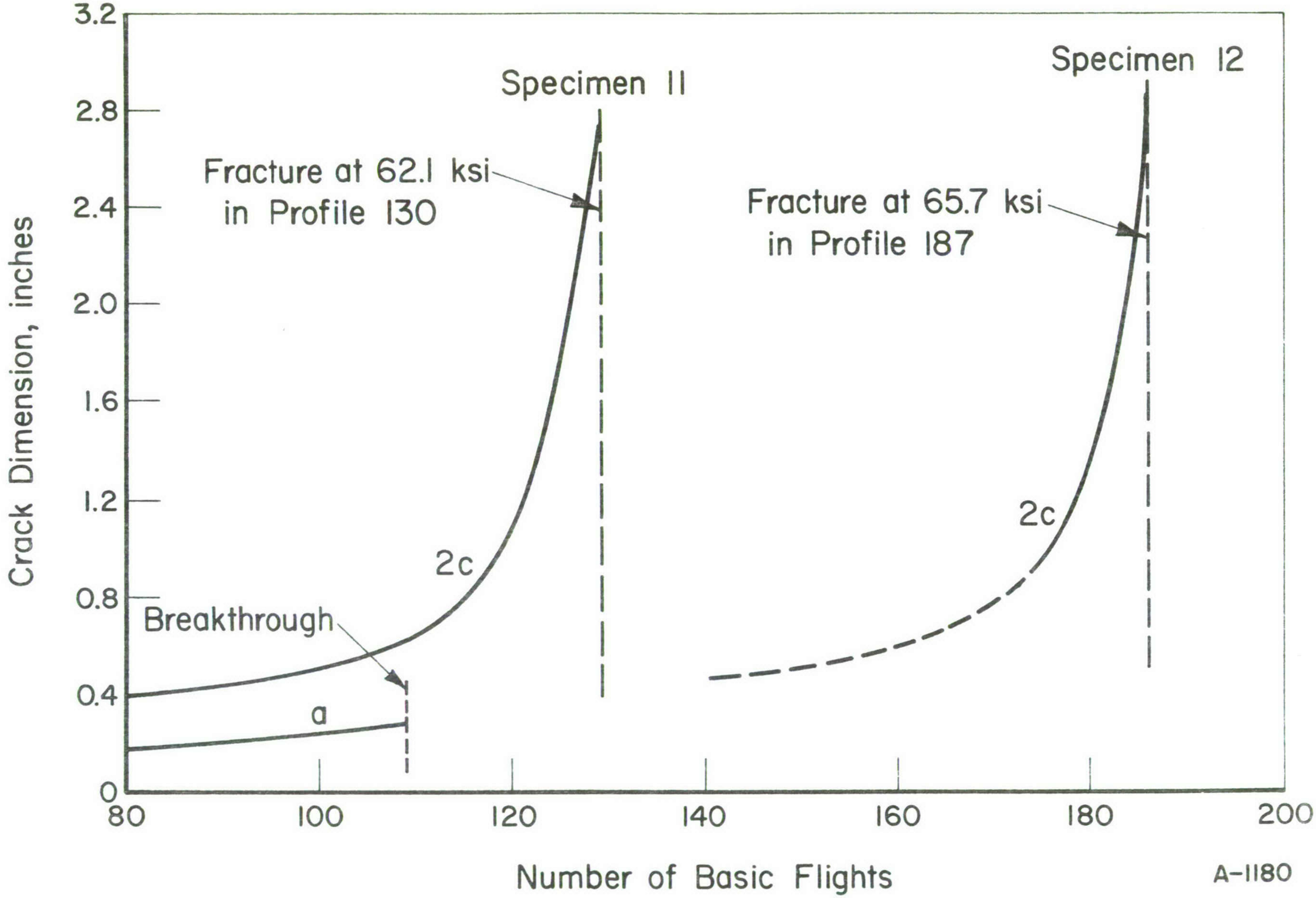

FIGURE B-7. CRACK GROWTH IN 3g FB SPECTRUM IN DESICCATED AIR AND JP-4

TABLE B-VIII. STRIATION MEASUREMENTS FOR SPECIMEN 12

Load Profile No.	Crack Depth a inch	Maximum Crack Length 2c inch	Remarks
	Striations Prior to Breakthrough of Surface Crack Obliterated		
174	---	.88	
175	---	.94	
176	---	.98	
177	---	1.05	
178	---	1.13	
179	---	1.22	
180	---	1.36	
181	---	1.50	
182	---	1.64	
183	---	1.80	
184	---	2.04	
185	---	2.40	
186	---	2.86	
187	---	3.02	Fracture

DISTRIBUTION LIST

Professor Holt Ashley
Department of Aeronautics & Astronautics
Stanford University
Room 546
Palo Alto, California 94305

Mr. Philip Donley
Flight Mechanics & Technology Div.
Langley Research Center
Hampton, Virginia 23365

Mr. William L. Gray
M.S. 10-47
The Boeing Company
P. O. Box 3707
Seattle, Washington 98124

Dr. Francis Hung
Executive Offices, L.A. Div.
North American Rockwell Corp.
1700 E. Imperial Hi-Way
El Segundo, California 90245

Dr. George Kendall
Aerospace Corporation
P. O. Box 95085
Los Angeles, California 90045

Air Force Materials Laboratory
Attention Dr. Alan M. Lovelace, Director
Wright-Patterson Air Force Base, Ohio 45433

Air Force Flight Dynamics Laboratory
Attention Mr. Hollan B. Lowndes, Jr., FB
Wright-Patterson Air Force Base, Ohio 45433

Mr. Herman Pusin
Director, Engineering
Aerospace Headquarters
Martin-Marietta Corp.
Friendship International Airport
Maryland 21240

Mr. Robert Rosenbaum
Federal Aviation Agency
SS-110
800 Independence Avenue, S.W.
Washington, D. C. 20590

Dr. Hassel C. Schjelderup
Dept. C1-20
Douglas Aircraft Company
3855 Lakewood Boulevard
Long Beach, California 90801

Mr. William T. Shuler
Chief, Structural Engineering
Dept. 72-01
Lockheed Georgia Company
Marietta, Georgia 20060

Mr. Donald E. Strand
M.S. 21-34
The Boeing Company
P. O. Box 3955
Seattle, Washington 98124

Aeronautical Systems Division
Attention Mr. Charles Tiffany, ENF
Airframe Subsystems
Engineering Directorate
Wright-Patterson Air Force Base,
Ohio 45433

General Dynamics Corporation
Attention Mr. William Dietz
Fort Worth, Texas 76101

Battelle Memorial Institute
Attention C. Feddersen
505 King Avenue
Columbus, Ohio 43201

Aeronautical Systems Division
Attention Mr. T. J. Keating, ENYX-L
F-111 SPO
Wright-Patterson Air Force Base,
Ohio 45433

Aeronautical Systems Division
Attention Mr. R. Wylan, ENYX-LF
F-111 SPO
Wright-Patterson Air Force Base,
Ohio 45433

Headquarters, U.S. Air Force
Attention Dr. J. W. Mar, AFCCN
Washington, D. C. 20330

Dr. Paul Packman
P. O. Box 3245, Sta. B
Vanderbilt University
Nashville, Tennessee 37205

Mr. Dale Little
General Dynamics Corporation
F-111 Engineering Project Office
P. O. Box 748
Fort Worth, Texas 76101

Dr. Alan Patching
Convair Aerospace Division
Mail Zone 1108
P. O. Box 748
Fort Worth, Texas 76101

Flight Dynamics Laboratory
Attention Mr. H. Wood, FB
Wright-Patterson Air Force Base, Ohio 45433

Air Force Materials Laboratory
Attention Mr. C. L. Harmsworth, LAE
Wright-Patterson Air Force Base,
Ohio 45433 (10

Dr. James C. Newman
Langley Research Center
National Aeronautics and Space Agency
Hampton, Virginia 23365

4950/TZDE
Wright-Patterson Air Force Base,
Ohio 45433

Air University Library
Maxwell Air Force Base, Alabama 3611[illegible]

Defense Documentation Center
Defense Supply Agency
Cameron Station
Alexandria, Virginia 22314 (12)

Unclassified
Security Classification

DOCUMENT CONTROL DATA - R & D

(Security classification of title, body of abstract and indexing annotation must be entered when the overall report is classified)

1. ORIGINATING ACTIVITY *(Corporate author)* Battelle's Columbus Laboratories 505 King Avenue Columbus, Ohio 43201	2a. REPORT SECURITY CLASSIFICATION Unclassified 2b. GROUP

3. REPORT TITLE

FATIGUE-CRACK PROPAGATION IN D6AC STEEL PLATE FOR SEVERAL FLIGHT LOADING PROFILES IN DRY AIR AND JP-4 FUEL ENVIRONMENTS

4. DESCRIPTIVE NOTES *(Type of report and inclusive dates)*
Final Report – February, 1971 – October, 1971

5. AUTHOR(S) *(First name, middle initial, last name)*

Charles E. Feddersen

6. REPORT DATE	7a. TOTAL NO. OF PAGES	7b. NO. OF REFS
January 28, 1972	72	17

8a. CONTRACT OR GRANT NO. F33615-71-C-1054, Subcontract 71-5 b. PROJECT NO. c. d.	9a. ORIGINATOR'S REPORT NUMBER(S) G-1101 9b. OTHER REPORT NO(S) *(Any other numbers that may be assigned this report)* AFML-TR-72-20

10. DISTRIBUTION STATEMENT

Approved for public release, distribution unlimited

11. SUPPLEMENTARY NOTES	12. SPONSORING MILITARY ACTIVITY
	Air Force Materials Laboratory Air Force Systems Command Wright-Patterson Air Force Base, Ohio

13. ABSTRACT

The objective of this experimental program was to obtain an independent evaluation of the fatigue-crack propagation characteristics of D6AC steel for the F-111 aircraft under specific flight loading spectra. The program also included selected studies of constant amplitude fatigue-crack propagation and crack growth retardation under the influence of single overloads.

It was determined that fatigue crack propagation specimens evaluated under spectra with peak loads exceeding one-half of the tensile yield strength of the material sustained significantly longer lifetime than under spectra wherein the peak loads were significantly below this stress level. Although the observations were limited, an effect of maximum cyclic stress on constant amplitude crack growth rates was apparent. In the crack growth retardation studies, it was observed that the overload ratio plays a direct role, and the maximum cyclic stress level an inverse role, in delaying crack growth.

Prediction of crack growth curves for variable amplitude flight profile loadings was attempted using various crack growth rate integration routines on constant amplitude fatigue crack propagation data. It was noted that a more meaningful appraisal and comparison of loading spectra could be achieved by a rate analysis of crack growth in terms of flight profiles rather than by the prediction of a crack growth in terms of retardation parameter strongly influenced both by initial crack size and by terminal toughness.

DD FORM 1 NOV 65 1473

Security Classification

Unclassified

Security Classification

14. KEY WORDS	LINK A		LINK B		LINK C	
	ROLE	WT	ROLE	WT	ROLE	WT
D6AC Steel						
Crack Growth						
Fatigue Crack Propagation						
Variable Amplitude Cyclic Loading						
Crack Growth Retardation						

Security Classification